



## RESEARCH ARTICLE

# Saturated areas through the lens: 1. Spatio-temporal variability of surface saturation documented through thermal infrared imagery

Marta Antonelli<sup>1,2</sup>  | Barbara Glaser<sup>2,3</sup> | Adriaan J. Teuling<sup>1</sup> | Julian Klaus<sup>2</sup> | Laurent Pfister<sup>2</sup> 

<sup>1</sup>Hydrology and Quantitative Water Management Group, Wageningen University & Research, Wageningen, The Netherlands

<sup>2</sup>Catchment and Eco-Hydrology Research Group, Luxembourg Institute of Science and Technology, Esch/Alzette, Luxembourg

<sup>3</sup>Department of Hydrology, University of Bayreuth, Bayreuth, Germany

## Correspondence

Marta Antonelli, Hydrology and Quantitative Water Management Group, Wageningen University & Research, Wageningen 6700, The Netherlands.

Email: marta.antonelli88@gmail.com

## Funding information

Luxembourg National Research Fund, Grant/Award Number: 10189601; FP7 People: Marie-Curie Actions, Grant/Award Number: 607150

## Abstract

Surface saturated areas are key features in generating run-off. A detailed characterization of the expansion and contraction of surface saturation in riparian zones and its connectivity to the stream is fundamental to improve our understanding of the spatial and temporal variability of streamflow generation processes. In this first contribution of a series of two papers, we used ground-based thermal infrared imagery for characterizing riparian surface saturation seasonal dynamics of seven different riparian areas in the Weierbach catchment (0.42 km<sup>2</sup>), a small forested catchment in Luxembourg. We collected biweekly panoramic images of the seven areas over a period of 2 years. We identified the extension of saturation in each collected panoramic image (i.e., percentage of pixels corresponding to saturated surfaces in each riparian area) to generate time series of surface saturation. Riparian surface saturation in all areas was seasonally variable, and its dynamics were in accordance with lower hillslope groundwater level fluctuations. Surface saturation in the different areas related to catchment outlet discharge through power law relationships. Differences in these relationships for different areas could be associated with the location of the areas along the stream network and to a possible influence of local riparian morphology on the development of surface saturation, suggesting a certain degree of intracatchment heterogeneity. This study paves the way for a subsequent investigation of the spatio-temporal variability of streamflow generation in the catchment, presented in our second contribution.

## KEYWORDS

catchment hydrology, ground-based thermal infrared imagery, intracatchment variability, remote sensing, riparian processes, surface saturation dynamics, surface saturation mapping

## 1 | INTRODUCTION

Saturation-excess overland flow and its connection to saturated areas were first documented in the seminal work by Dunne and Black

(1970). Surface saturated areas (i.e., areas presenting water at the ground surface) have been recognized as key areas for mediating the onset and offset of hydrological connectivity between hillslopes and streams in humid temperate environments (Ambroise, 2004; Birkel,

This is an open access article under the terms of the Creative Commons Attribution License, which permits use, distribution and reproduction in any medium, provided the original work is properly cited.

© 2020 Luxembourg Institute of Science and Technology. *Hydrological Processes* published by John Wiley & Sons Ltd.

Tetzlaff, Dunn, & Soulsby, 2010; Bracken & Croke, 2007; Hewlett, 1961; Tetzlaff et al., 2007). Saturation dynamics and the associated hydrological connectivity have been on the agenda of both modelling and experimental studies. Many monitoring studies of surface saturation focused on the near-stream area (i.e., riparian area), which is particularly relevant for run-off generation due to its intrinsic proximity to the stream. Several studies have shown that the spatial extent of near-stream surface saturated areas is a valuable indicator of the general hydrological state of the catchment and, in particular, of groundwater storage during baseflow conditions (i.e., Ambroise, 2016; Gburek & Sharpley, 1998; Myrabø, 1997). During precipitation events, riparian surface saturated areas can quickly extend and convey event water to the stream and act as mixing areas for hillslope water contributions (Soulsby, Birkel, & Tetzlaff, 2016; Tetzlaff, Birkel, Dick, Geris, & Soulsby, 2014; Weill et al., 2013). This is often observed in catchments characterized by confined valley bottoms, where persistent saturation can develop in riparian locations with low relief and a shallow water table (Dunne, Moore, & Taylor, 1975; Niedda & Pirastu, 2014). Thus, an accurate characterization of expansion and contraction dynamics of riparian surface saturation is needed to fully interpret the hydrological behaviour of catchments exhibiting these features and to accurately predict run-off dynamics and associated water and nutrient flowpaths.

Varying riparian morphological traits and upland topographic characteristics have been associated to the variability in hydrological and biogeochemical functions of riparian zones. Several studies have accounted for the spatial variability of riparian zones when exploring riparian functions such as water table fluctuation (Grabs, Bishop, Laudon, Lyon, & Seibert, 2012), vertical and lateral connectivity (Leach et al., 2017; Ploum, Leach, Kuglerová, & Laudon, 2018), or water travel distance and retention of chemicals (Grabs et al., 2012; Ledesma et al., 2018; Roulet, 1990; Vidon & Hill, 2004). On the other hand, riparian surface saturation dynamics have been mainly investigated by taking into account single riparian sections (Zillgens, Merz, Kirnbauer, & Tilch, 2007) or the dynamics of the riparian system as a whole (Ocampo, Oldham, Sivapalan, & Turner, 2006). Due to the spatial variability of riparian characteristics (i.e., riparian width, slope, and soil depth), monitoring of surface saturation that is restricted to a single riparian section can be far from being representative of the whole catchment's riparian zone. Similarly, mapping the dynamics of surface saturation of the riparian zone as a whole may conceal important small-scale variability. Therefore, it is fundamental to characterize riparian surface saturation by accounting for riparian zones' spatial heterogeneity.

As early as in 1975, Dunne et al. made a call for the development of a routine method for the "recognition and quantification of the seasonal and in-storm [and inter-storm] variation of the saturated runoff-producing zones." Progress towards a routine method for mapping the spatio-temporal variability of saturated areas in humid environments remains hampered by technological limitations, especially when it comes to mapping surface saturation dynamics with high spatial and temporal resolutions. In order to get a better understanding of the spatial and temporal scales at which previous studies have addressed

surface saturation, we reviewed a total of 64 studies on surface saturation. In 25 of the reviewed studies, surface saturation dynamics were estimated through the use of proxies for surface saturation such as riparian water table level variations (e.g., Waddington et al., 1993; Vidon & Hill, 2004; Ocampo et al., 2006; Tetzlaff et al., 2014), modelling approaches (e.g., Appels, Bogaart, & van der Zee, 2016; Beven & Kirkby, 1979; Blumstock, Tetzlaff, Dick, Nuetzmann, & Soulsby, 2016; Dick, Tetzlaff, Birkel, & Soulsby, 2015; O'Loughlin, 1987; Weill et al., 2013), or a combination of the two (e.g., Baker, Wiley, & Seelbach, 2001; Frei, Lischeid, & Fleckenstein, 2010; Myrabø, 1997; Stieglitz, 2003; von Freyberg, Radny, Gall, & Schirmer, 2014). Proxies for surface saturation such as water table dynamics can be collected at high temporal resolution but are limited to punctual spatial observations. Modelling approaches for estimating surface saturation dynamics commonly rely on the estimation of topography-based wetness such as the topographic wetness index employed in TOPMODEL (Beven & Kirkby, 1979), multiple existing topographic wetness index variants, or geomorphic indices (Ali et al., 2013). These models allow for an estimation of surface saturation over large spatial extents (up to hundreds of km<sup>2</sup>). However, some of the models' underlying assumptions may not always be valid (e.g., the local slope may not be a valid proxy of the downslope hydraulic gradient), especially in catchments of flat terrain (Grabs, Seibert, Bishop, & Laudon, 2009; Rodhe & Seibert, 1999). Other modelling studies relied on spatially distributed, physically based simulations of surface saturation dynamics (e.g., Frei et al., 2010; Weill et al., 2013), yet these studies lacked a detailed assessment of the validity of the model results against field observations.

Direct mapping of surface saturation (rather than relying on the use of proxies or modelling) was performed within 30 of the 64 reviewed studies for varying spatial extents and with varying monitoring frequencies (Figure 1 provides a graphical representation of the space-time sampling characteristics of surface saturation mapping from these 30 studies, plus this contribution). Except for a few exceptions (i.e., Birkel et al., 2010; Coles & McDonnell, 2018; Tanaka, Yasuhara, Sakai, & Marui, 1988), field surveys (e.g., squishy boot method) have been applied for mapping areas below 5 km<sup>2</sup> and at low temporal resolution (i.e., mainly monthly and punctual observations). Saturation mapping via remote sensing tools has been mainly relying on satellite and airborne platforms. These techniques are less labour-intensive compared with field surveys and can deliver a higher amount of observations in a certain time frame and for larger areas (i.e., > 5 km<sup>2</sup>; de Alwis, Easton, Dahlke, Philpot, & Steenhuis, 2007; Mengistu & Spence, 2016; Phillips, Spence, & Pomeroy, 2011). However, similar to field surveys, remote sensing observations from satellite platforms do not provide the necessary spatial and temporal resolution for detecting heterogeneous riparian surface saturation dynamics within a catchment. Ground-based remote sensing techniques (i.e., thermal infrared [TIR] or visible light imagery) can provide observations at higher temporal (i.e., minutes to weeks) and spatial (i.e., centimetres to meters) resolutions (Glaser et al., 2016; Pfister, McDonnell, Hissler, & Hoffmann, 2010; Silasari, Parajka, Ressler, Strauss, & Blöschl, 2017). These techniques will likely become pivotal in generating new, more detailed insights into the functioning of

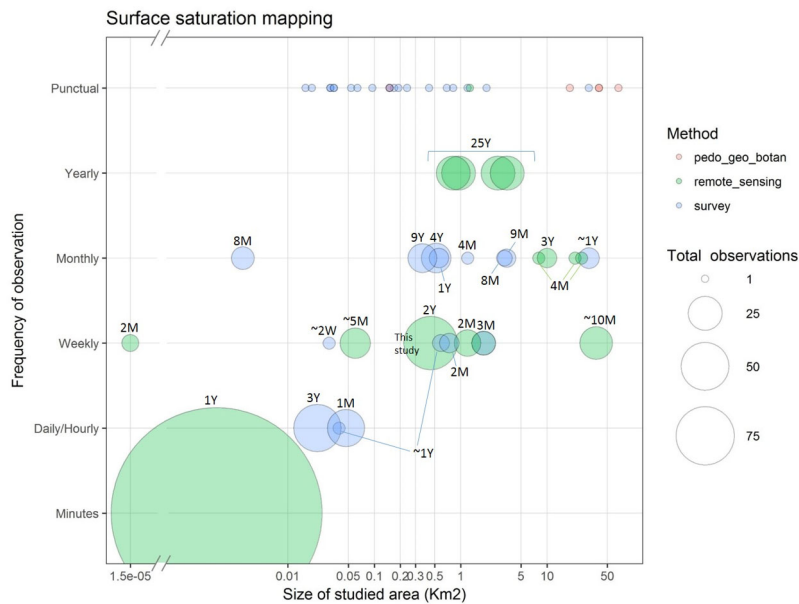


**FIGURE 1** Space–time sampling characteristics of surface saturation mapping from 30 different studies that employed direct mapping of surface saturation, plus this contribution. The size of the studied area refers to the overall area of the investigated catchment or hillslope and the quantity value refers to the total number of times the area has been mapped (information acquired but not directly used in the publication has been included). Studies where different surface saturation mapping methods have been employed or where the same method was employed for different areas have been considered as multiple examples. Methods are indicated with “survey” (e.g., squishy boots method), “remote sensing” (e.g., ground-based and satellite), and “pedo-geo-botan” (i.e., pedological, geological, and botanical aspects used to delineate permanently surface saturated areas of the catchment). The total duration of the mapping period is indicated close to the circles for nonpoint observations (Y = years, M = months, W = weeks). In order to make the studies comparable in terms of surface saturation frequency of observation, we considered only the most recurrent time interval between two observations for each study. Studies that reported a seasonal mapping were included under the monthly frequency. Note that the big circle (which corresponds to a year of digital images acquired every minute during day time by Silasari et al., 2017) is not in scale for display purposes. References for the 30 studies considered for the review figure: Ali et al., 2013; Ambroise, 2016; Bari, Smettem, & Sivapalan, 2005; Birkel et al., 2010; Blazkova, Beven, & Kulasova, 2002; Brun et al., 1990; Buttle & Sami, 1992; Chabot & Bird, 2014; Coles & McDonnell, 2018; Creed, Sanford, Beall, Molot, & Dillon, 2003; D. A. De Alwis, Easton, Dahlke, Philpot, & Steenhuis, 2007; Devito, Creed, & Fraser, 2005; Dunne et al., 1975; Franks, Gineste, Beven, & Merot, 1998; Gineste, Puech, & Mérot, 1998; Glaser et al., 2016; Grabs, Seibert, Bishop, & Laudon, 2009; A. Güntner, Uhlenbrook, Seibert, & Leibundgut, 1999; Andreas Güntner et al., 2004; Inamdar & Mitchell, 2007; Kulasova, Beven, Blazkova, Rezacova, & Cajthaml, 2014; Latron & Gallart, 2007; McDonnell & Taylor, 1987; Mengistu & Spence, 2016; Pfister et al., 2010; Phillips et al., 2011; Rinderer, Kollegger, Fischer, Stähli, & Seibert, 2012; Roulet, 1990; Silasari et al., 2017; Tanaka et al., 1988. The bibliography for the 30 studies considered for the review figure can be found in Appendix A1

surface saturated area variability and dynamics. Similarly to ground-based TIR, other techniques based on temperature detection (such as thermal imagery from unmanned aerial vehicles and fibre optic distribute temperature sensing) can also provide observation at high spatial (i.e., centimetres to kilometres) and temporal (i.e., minutes to weeks) resolutions, although until today, they have been primarily employed for the characterization of longitudinal stream temperatures and detection of GW exfiltration (Briggs, Dawson, Holmquist-Johnson, Williams, & Lane, 2019; Selker, van de Giesen, Westhoff, Luxembourg, & Parlange, 2006). Within the 64 reviewed studies, 11 did not report clear information on the spatial and temporal scales at which surface saturation was addressed.

Here, we analyse the temporal variability of different riparian surface saturated areas under a new resolution and perspective—namely, “through the lens” of a TIR camera. We employed ground-based TIR imagery in an analogous approach to Pfister et al. (2010) and Glaser et al. (2018; 2016; i.e., to detect temperature differences between the water at the ground surface—saturated areas—and the surrounding

environment—unsaturated areas), to obtain a unique dataset of 2 years of biweekly observations of different riparian surface saturated areas within the Weierbach catchment in Luxembourg. This long-term studied headwater catchment (0.42 km<sup>2</sup>) is a reference site for rainfall-dominated mountainous catchments (Zuecco, Penna, & Borga, 2018). The Weierbach is characterized by homogeneous pedology and geology and exhibits a hydrological response that is highly influenced by the wetness state of the system. This leads to a single-peak response during dry conditions and a double-peak response during wet conditions—after a threshold in catchment storage is exceeded (Martínez-Carreras et al., 2016). The Weierbach catchment has a well-developed riparian zone, characterized by variable morphology (e.g., riparian width and elevation) and the presence of perennial and/or temporary groundwater exfiltration points. Although there is a reasonable understanding of how the overall hydrological response of the catchment is generated (Fenicia et al., 2014; Glaser et al., 2016; Klaus, Wetzel, Martínez-Carreras, Ector, & Pfister, 2015; Martínez-Carreras et al., 2016; Schwab, Klaus, Pfister, & Weiler, 2018; Wrede

et al., 2015), there is still a lack of understanding of the dynamics of small-scale riparian processes, like the spatial and temporal variability of riparian surface saturation, and of how these dynamics are related to the hydrological response (Scaini et al., 2017).

In this first contribution of a series of two papers, we apply ground-based TIR imagery as a routine method for mapping surface saturation dynamics across multiple seasonal and hydrological conditions and across multiple sites in the riparian zone of the Weierbach catchment. We analyse the spatio-temporal dynamics of surface saturation by applying statistical analyses on an extensive surface saturation dataset produced by direct field observation. In particular, through this novel approach, we investigate the following questions on saturated area dynamics:

1. Are the overall surface saturation dynamics (i.e., seasonal and yearly dynamics) of the seven investigated areas similar?
2. How do hydrological conditions (i.e., precipitation, stream discharge, evapotranspiration, groundwater level, soil moisture, and catchment storage) relate to the temporal (seasonal and yearly) variability of surface saturation in different riparian locations in a catchment?

We leverage the outcomes of this study in the accompanying manuscript for investigating how hillslope–riparian–stream (HRS) connectivity is established in the Weierbach catchment. This will eventually improve our understanding of how the spatial variability of streamflow generation is linked to surface saturation dynamics.

## 2 | STUDY SITE—THE WEIERBACH CATCHMENT

The Weierbach experimental catchment (0.42 km<sup>2</sup>) is located in North-West Luxembourg (49°49'N, 5°47'E; Figure 2). The climate is semiocenic, with an annual average precipitation of 918 mm

(2011–2017). Precipitation is rather evenly distributed throughout the year, whereas streamflow is lowest from May to September, mainly due to evapotranspiration losses. Pedology and geology are quite homogeneous throughout the catchment. Slate-dominated bedrock is fractured from 1.4- to 5-m depth. Soil consists of a thin organic topsoil (approximately first 5 cm) above a sandy-loamy *solum* (up to 50-cm depth) and *subsolum* (from 50- to 140-cm depth) characterized by rock fragments, which volumetric portion increases with depth from 25% in the *solum* to more than 80% in the deeper fraction of the *subsolum* (Gourdol, Clément, Juilleret, Pfister, & Hissler, 2018; Juilleret, Iffly, Pfister, & Hissler, 2011). Drainage porosity decreases from the *solum* (30% drainage porosity) to the *subsolum* (10% drainage porosity; Gourdol et al., 2018).

Elevation ranges from 458 to 513 m.a.s.l. Topography is characterized by a quasihorizontal plateau, covering 54% of the catchment and cut by steep ( $\geq 5^\circ$ ) V-shaped valleys.

Vegetation is composed of Oak and Beech trees on the western side of the catchment and Spruce on the eastern side. Ferns and herbaceous plants dominate in the riparian zone. In this study, we identify the riparian zone considering a combination of different criteria. The change in dominant vegetation and the presence of shallow clay-loam, organic soil (i.e., Leptosol), peculiar of the low relief near-stream area of the catchment, set a visual basis for differentiating riparian from other landscape elements (i.e., hillslopes, plateau). The riparian zone is gently sloped ( $< 5^\circ$ ) and covers 1.2% of total catchment area.

The catchment's run-off response to precipitation is influenced by a storage threshold (Martínez-Carreras et al., 2016) and changes between the dry and the wet seasons. In case of dry antecedent conditions, the catchment produces a single spiky peak of short duration (i.e., hours), whereas the response is bimodal during wet antecedent conditions—with a first peak followed by a broader second peak of longer duration (extending up to several days). Martínez-Carreras et al. (2016) showed that the first peak is mainly composed of water from precipitation, throughfall, and rapid HRS connectivity through

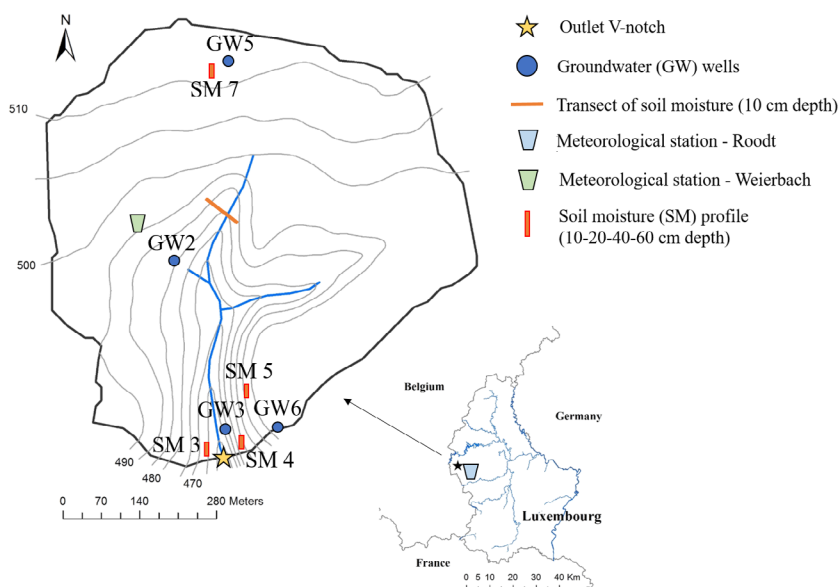


**FIGURE 2** Location and instrumentation map of the Weierbach catchment



saturation excess overland flow and preferential flowpaths (such as macropores and/or fractures along the hillslopes) whereas the second peak mainly consists of infiltrated soil water and groundwater flowing through the fractured bedrock, once the storage threshold is exceeded.

### 3 | MATERIALS AND METHODS

#### 3.1 | Hydrometeorological measurements and catchment storage calculation

Hydrometeorological measurements are carried out in the Weierbach catchment since 2002 as part of a long-term monitoring programme. Water levels were measured and recorded every 15 min by a pressure transducer (ISCO 4120 Flow Logger) installed at a V-notch weir at the catchment outlet (Figure 2) and translated into discharge via a rating curve (based on salt dilution measurements). Precipitation data were measured at a canopy-free location in the Weierbach catchment (see Figure 2) and recorded every 5 min with a tipping bucket (Young, model 52203, connected to a Campbell logger CR200X). At the same location, air temperature and relative air humidity were monitored. These data were combined with readings from a meteorological station in Roodt (about 3.5 km from the catchment) to calculate the reference evapotranspiration (ET<sub>0</sub>) following the FAO Penman-Monteith equation (Allen, Pereira, Raes, Smith, & Ab, 1998).

Ground water (GW) levels were measured every 15 min in four piezometers: GW2 (2.00-m depth, screened for the last lower 1.36 m) and GW3 (2.35-m depth, screened for the last lower 1.60 m) placed along a hillslope, and GW5 (7.57-m depth, screened for the last lower 3.82 m) and GW6 (4.85-m depth, screened for the last lower 3.50 m) located on the plateau (Figure 2).

Volumetric soil water content (VWC) was measured in the shallow soil every 15 min using a Campbell CS616 sensor installed at 10-cm depth along a transect through the HRS continuum (Figure 2, soil moisture transect), covering the west upslope (Beech covered), midhillslope, foot of the hillslope, riparian zone, and east upslope (Spruce covered). Additionally, soil VWC was measured every 30 min using Campbell CS650 sensors installed at 10-, 20-, 40-, and 60-cm depth in four sites (Figure 2, soil moisture sites 3, 4, 5, and 7). Sites 3 and 4 are placed at low hillslope positions (Beech covered and Spruce covered, respectively), Site 5 is placed at midhillslope position (Pines covered), and Site 7 is placed on the plateau (Beech covered).

Catchment storage estimates were calculated following the methodology developed by Martínez-Carreras et al. (2016). In their study, the total amount of water stored in the catchment at a given time was calculated as the sum of storage in three separate zones:

$$S_{\text{TOTAL}} = S_{\text{UNSAT}} + S_{\text{SAT}} + S_{\text{RES}}$$

where  $S_{\text{UNSAT}}$  is the water stored in the variably unsaturated zone (estimated from the VWC of the soil above the water content at field capacity—measured at the different soil depths in Sites 3, 4, 5, and 7),

$S_{\text{SAT}}$  is the water stored in the variably saturated zone (within the range of water table fluctuations—estimated from GW levels in the hillslope and in the plateau: GW3 and GW5, respectively, in this study), and  $S_{\text{RES}}$  is the water stored in the residual saturated zone (i.e., estimated drainage porosity of the basal layer, fractured bedrock, and fresh bedrock).  $S_{\text{TOTAL}}$  is obtained for the different landscape elements by multiplying the value of total storage by the area of each element. For more specific information on the calculation of catchment storage, the reader is referred to Martínez-Carreras et al. (2016).

#### 3.2 | Monitoring of surface saturated areas in the riparian zone

We focused on seven distinct riparian areas in the Weierbach catchment (Figure 3). Each area was labelled with an abbreviation (cf. areas' name in Figure 3) indicating the stream branch where it is located (i.e., L = riparian areas on the left stream branch; M = riparian areas on the middle branch; R = riparian areas on the right branch, and S = riparian areas on the main stream) and its position along the branch (i.e., numbered from downstream to upstream). Descriptive topographic characteristics of the different riparian areas, such as average elevation, area extension (i.e., area covered by the monitoring), and maximum riparian width, were extracted from a high resolution LIDAR DEM (~5-cm resolution). TIR observations (i.e., sequential images and videos) and visible light photographs of the different riparian areas were acquired for a total of 63 mapping campaigns with a weekly to fortnightly recurrence interval from November 2015 to December 2017. The used handheld TIR camera (FLIR T640, FLIR Systems, Wilsonville, OR, USA) is sensitive to the radiation emitted from an observed surface (or the first 0.1 mm of a water column) over a spectral range of 7.5 to 14  $\mu\text{m}$ , produces images of 640  $\times$  480 pixels, and covers a temperature range of  $-40^{\circ}\text{C}$  to  $2000^{\circ}\text{C}$ , with a thermal sensitivity of  $<0.035^{\circ}\text{C}$  at  $30^{\circ}\text{C}$ . Information about object emissivity " $\epsilon$ " (usually set between 0.95 and 0.97 for freshwater), atmospheric temperature, air humidity, object's distance from the device, and reflected ambient temperature were provided to the camera in order to correct the detected temperature for these parameters (the correction is automatically done by the camera's software).

The final product of the TIR camera is an image (or video) reporting surface temperatures for each image pixel. This temperature information can be used to classify the pixels into pixels corresponding to water ponding or flowing at the ground surface (saturated pixels, i.e., stream and riparian ponds) and pixels representing surrounding material (unsaturated pixels, i.e., soil, rock, and vegetation; Figure 4a,b). In order to be able to discern these two pixel classes, a clear temperature contrast between surface water (saturated pixels) and surrounding material (unsaturated pixels) is required. Moreover, the camera view on the saturated surfaces has to be free from obstructions (e.g., vegetation, snow, fog, and heavy rain). Below, we shortly explain how we transformed the information from the acquired TIR images into information on the extent of surface

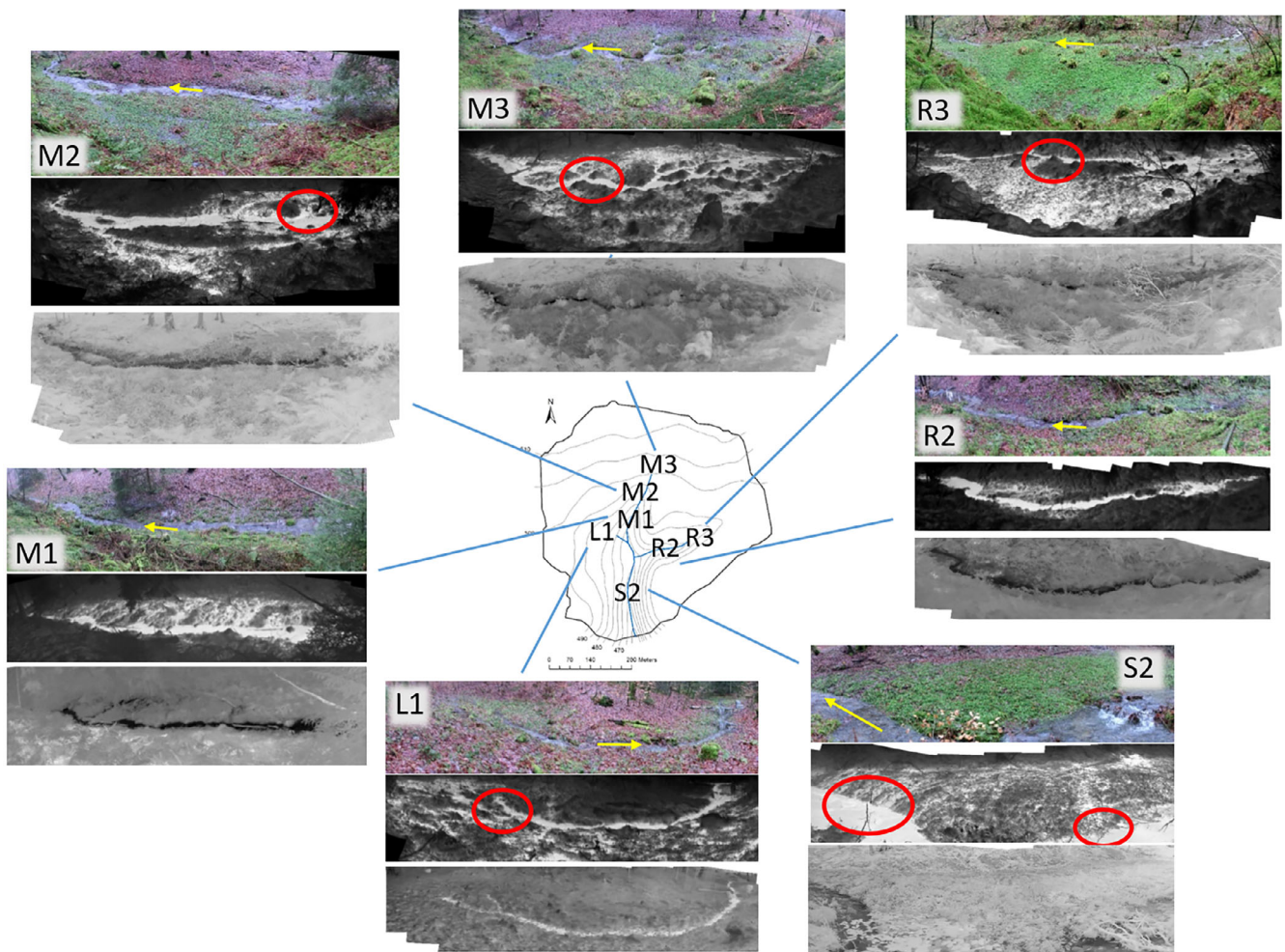


**FIGURE 3** Location and example of visible light and thermal infrared (TIR) panoramic photo of each investigated riparian area for a wet and dry condition. Visible light images are shown for wet conditions only. In the TIR panoramas collected during wet conditions, saturated pixels correspond to the lighter colours. In the TIR panoramas collected during dry conditions, saturated pixels correspond to the darker colours (except for Area L1; pictures: M. Antonelli and B. Glaser). Yellow arrow: flow direction. Red circles: location of permanent springs

saturation. A detailed description of the postprocessing workflow and the TIR imagery technique applied for surface saturation mapping in general can be found in Glaser et al. (2018).

In order to prepare the TIR images (or videos) for the extraction of the extent of surface saturation in the investigated riparian areas, we followed a sequence of postprocessing steps. The sequence consisted of (a) creating panoramic images by overlapping single images (or video frames; Figure 4a,d), (b) transforming all panoramas from the same area into the same perspective by coreferencing them to a selected reference panorama, and (c) cropping all images to the same area of interest. For more details on the postprocessing steps, we refer to fig. 3 in Glaser et al. (2018), where the methodology for the TIR approach was developed. We then calculated the percentage of saturated pixels in each panorama as proxy for the extent of surface saturation in the investigated areas following the manual approach for the generation of saturation maps described in Glaser et al. (2018). This approach consists in (a) manually selecting the temperature range corresponding to surface saturation, (b) adapting the selected range to create a saturation map with a pattern of saturated

pixels matching best the saturation pattern identified via visual inspection of the TIR panoramas and visible light images (here defined as optimal solution), and (c) calculating the number of pixels falling into that temperature range over the total number of pixels of each image (Figure 4e). The three steps were repeated for each location and observation date, meaning that an individual temperature range was selected for each TIR panorama. TIR panoramas that showed poor temperature contrast and/or high influence from obstructing elements were excluded from the analyses (34% of the 441 acquired panoramas).

As shown by Glaser et al. (2018), the manual selection of temperature ranges is to date the best approach for generating reliable saturation maps from TIR datasets where images show very variable conditions (e.g., in terms of wetness and overall temperature range) and present slight perspective shifts. However, because the manual selection of an optimal solution for the saturation estimation is a subjective process, different operators may tend to select different optimal temperature ranges, including more or less pixels into the group of saturated pixels based on their individual perception.

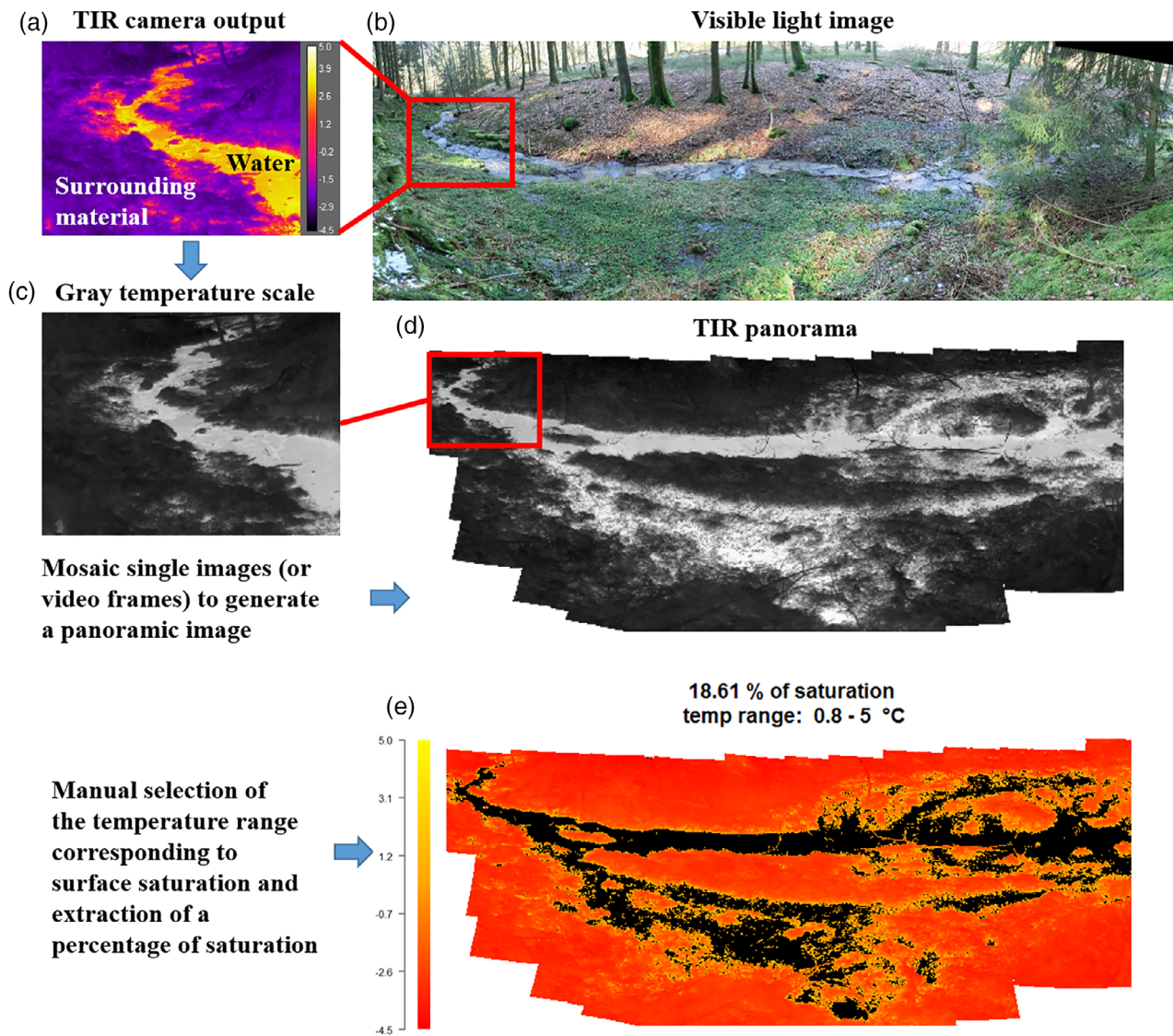


**FIGURE 4** Workflow of the thermal infrared (TIR) image postprocessing for the example of the TIR panorama of Area M2 of February 25, 2016. For more details, the reader is referred to Glaser et al. (2018)

To investigate the range of possible surface saturation outcomes, we varied for some panoramas the width of the saturated pixels temperature range (i.e., changing the higher and the lower values in small temperature steps) until the saturation pattern clearly mismatched the saturation pattern selected as the optimal solution (cf. Glaser et al., 2018). The saturation pattern including the higher number of pixels, and still reflecting the realistic saturation pattern, was used to determine the maximum estimate of surface saturation. The saturation pattern including the lower number of pixels, and still reflecting the realistic saturation pattern, was used to determine the minimum estimate of surface saturation. We estimated different saturation outcomes for the investigated riparian areas taking into account images collected during different saturation levels (i.e., five to seven images for each investigated area). We then plotted the minimum and maximum estimates of saturated pixels against the optimal estimation (within each area) and determined a regression equation from which

we retrieved the minimum and maximum estimates of saturation for the whole time series of saturation of each of the areas.

The overall amount of surface saturation estimated from the TIR images in each area represents both riparian surface saturation and water in the stream channel. The stream channel receives water contributions from the riparian zone (i.e., lateral contribution; cf. Figure 3 red circles) and water supply from upstream along the stream channel itself (i.e., longitudinal/upstream contribution). The relative amount of water provided by these two different contributions is difficult to disentangle. However, between the investigated riparian areas, we expect upstream contributions to be higher in downstream areas compared with headwater areas. In order to strengthen the comparison of the relationships between riparian surface saturation in different areas (i.e., headwater areas vs. downstream areas) and stream discharge (cf. Figure 11 in Section 4), we provide an example of an estimation of downstream areas' surface saturation with a reduced influence of the



upstream contribution (i.e., excluding the stream from the calculation of surface saturation). However, this exercise leads to a considerable loss of information on the overall level of surface saturation because, by doing so, a substantial part of surface water represented by the lateral inflows is also excluded. For this reason, the estimation of surface saturation with a reduced influence of the upstream contribution is only provided as an example, and it is not employed in all the analyses.

### 3.3 | Statistical data analysis

We analysed the time series of saturation of the seven riparian areas, in order to investigate the temporal dynamics of surface saturation. We applied a min–max normalization to the percentage of saturated

pixels for each area. We expressed the normalized values as a percentage in order to compare areas of different extension (cf. Section 4.1). We will refer to these values as “normalized saturation.” For the normalization, we accounted for the percentage of saturated pixels from images acquired during periods where surface saturation was not affected by particular meteorological conditions such as frozen soils (which will be represented by normalized percentages below 0%) or rain-on-snow events (which will be represented by normalized percentages above 100%). By quantifying the observations obtained during the occurrence of frozen soils and rain-on-snow events in this way, they can be easily identified in the figures and provide information on the field conditions. These observations were retained in the statistical analysis of the dataset because they are not statistical outliers. Nevertheless, we tested the statistics excluding

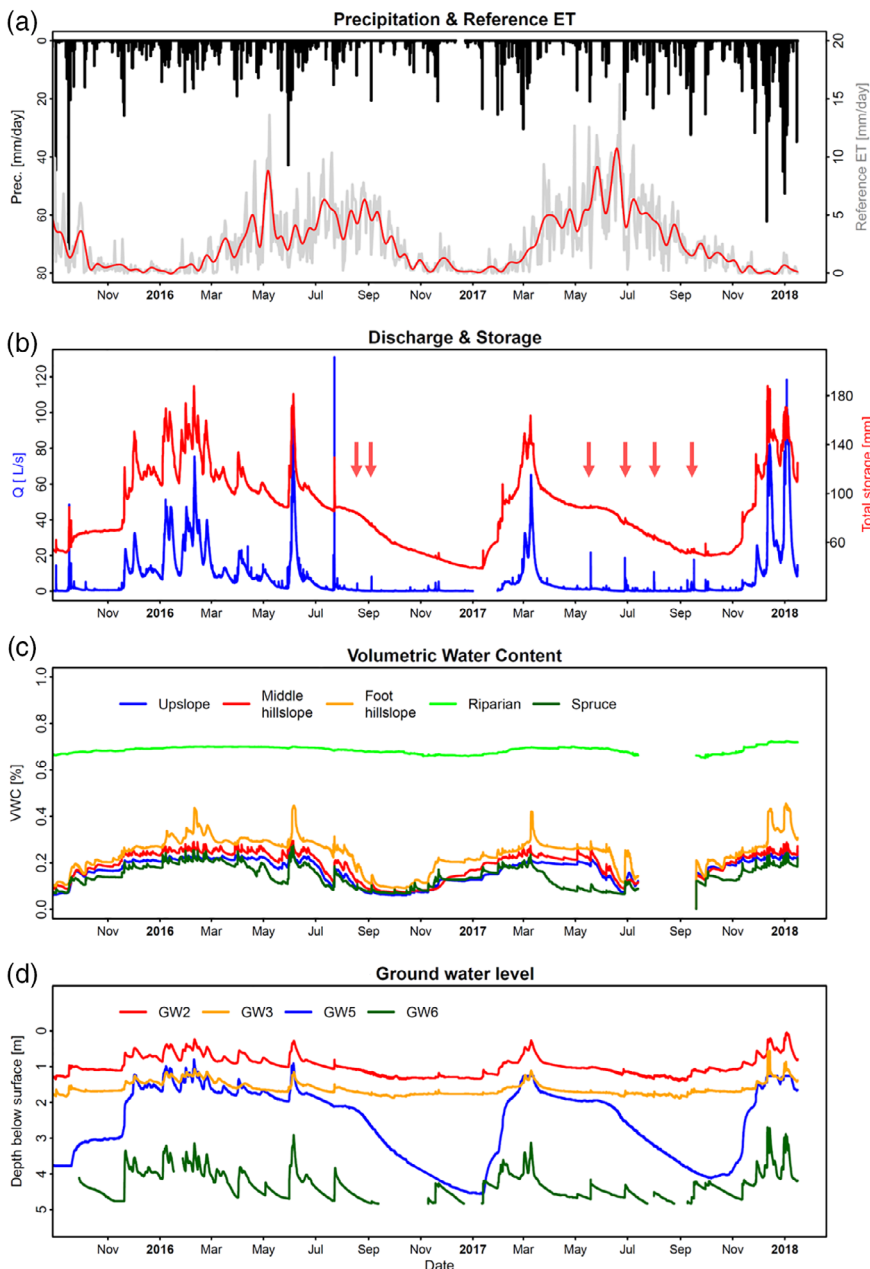


**FIGURE 5** Time series of (a) precipitation (black) and reference evapotranspiration (grey—smoothed trend of reference ET showed in red), (b) discharge and catchment storage (red arrows show moments when discharge response was more pronounced than catchment storage), (c) soil volumetric water content along the hillslope–riparian–stream transect (10-cm depth), and (d) ground water levels from October 2015 to January 2018

these observations and the results remained consistent. Descriptive statistics and the nonparametric Mann–Whitney–Wilcoxon Test ( $\alpha = .05$ ) were used to compare the temporal distribution of the normalized saturation in different areas.

In order to explore a possible influence of precipitation and evapotranspiration on the seasonal dynamics of surface saturation in the different areas, we compared the double mass curves (DMCs) of rainfall and run-off of the catchment for the two investigated hydrological years (HYs) with the DMCs of rainfall and surface saturation in the different areas (i.e., we cumulated the estimated values of normalized surface saturation from one date of observation to the other and highlighted moments of vegetation growth and high evapotranspiration). Classical rainfall–run-off DMCs can provide direct information on seasonal run-off formation (Pfister, Iffly, Hoffmann, & Humbert, 2002; Seibert, Jackisch, Ehret, Pfister, & Zehe, 2017). Similarly, by evaluating how cumulated surface saturation evolves in response to cumulated rainfall, we aimed to obtain information on the influence of seasonal variables (i.e., precipitation and evapotranspiration) on the development of surface saturation. Note that by cumulating normalized surface

saturation, we do not intend to give an estimation of a total amount of surface saturation of each HY. Instead, we consider the cumulated surface saturation as a way to identify periods of general increase or decrease of saturation.

As a measure of how fast the saturation changed in each area, we calculated the difference between the normalized saturation estimated on two consecutive dates and divided this value by the number of days in each period to obtain daily normalized rates of change. We tested similarities between the daily rates of change between different areas with the Mann–Whitney–Wilcoxon Test ( $\alpha = .05$ ). The test was applied by taking into account each surface saturated area against every other area for the dates when an estimation of a change rate of saturation was available for both areas. Additionally, we tested if the difference in normalized saturation estimated between two consecutive dates was related to differences in GW levels, soil VWC along the HRS transect and soil VWC profiles at Sites 3, 4, 5, and 7, catchment storage or to the amount of precipitation (expressed via the antecedent precipitation index—as per McDonnell, Owens, & Stewart, 1991) observed between the same dates. We applied Spearman's rank

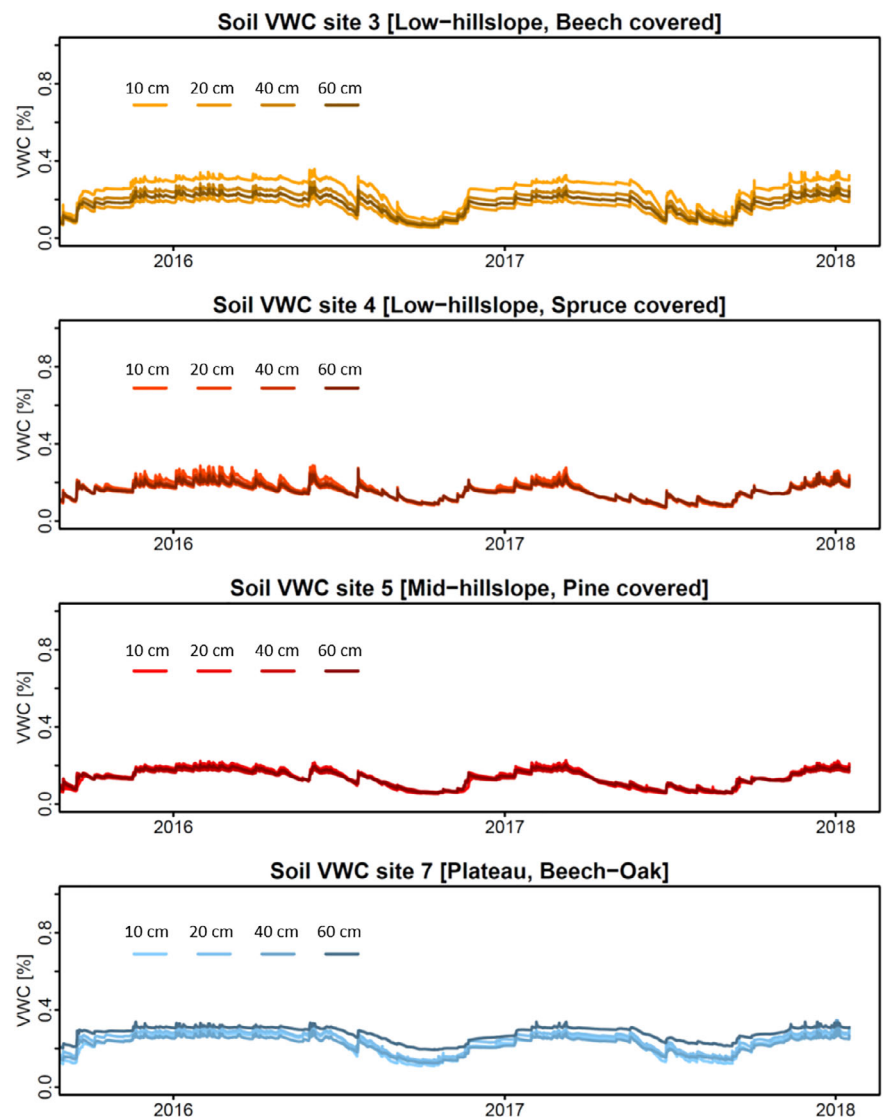


**FIGURE 6** Time series of soil volumetric water content measured at 10-, 20-, 40-, and 60-cm depth at Sites 3, 4, 5, and 7, from October 2015 to January 2018

correlation to test these relationships ( $\alpha = .01$ ). As before, we only took into account the dates for which an estimation of saturation was available for the analysed area.

We applied Spearman's rank correlation test rho ( $\rho$ ;  $\alpha = .01$ ) in order to test monotonic relationships between (a) the time series of normalized saturation estimated in the different investigated riparian areas and (b) between these values and the time series of hydrometric measurements (i.e., daily-averaged values of outlet discharge, estimated catchment storage, GW levels, soil VWC along the HRS transect, and soil VWC profiles at Sites 3, 4, 5, and 7). These relationships were tested for the whole study period.

In order to analyse the shape of the relationship between the surface saturation in the different areas and baseflow discharge at the catchment outlet, we relied on the observations of surface saturation that were not impacted by the occurrence of precipitation (i.e., images taken while rainfall occurred, during rising limbs or peaks of discharge, and at the early stage of discharge recession) or by the occurrence of particular meteorological conditions such as frozen soils or rain-on-snow events. This set of data describes the evolution of surface saturation along the gradual change in wetness state of the catchment and can be related to the surface saturation versus baseflow discharge relationship described by Ambroise (2016). We fitted various types of equations on the observations not impacted by the occurrence of

precipitation, and we found that power law equations ( $Sat = a \cdot Q^b$ ) adequately approximate the observed trends (fitting carried out on nontransformed data; goodness-of-fit was tested with Kolmogorov-Smirnov test— $p$  value  $>.1$ ).

## 4 | RESULTS

### 4.1 | Hydrological response and catchment storage

We monitored the hydrological response of the Weierbach catchment from November 2015 to December 2017 (Figure 5). Annual precipitation remained similar (921 and 913 mm/year) during the two monitored HYs (extending from October to September of the following year). Annual run-off was  $\sim 752$  and  $\sim 177$  mm/year for the HY 2015/2016 and 2016/2017, respectively. The particularly low run-off registered for the HY 2016/2017 may be explained by exceptionally low amounts of precipitation during the beginning of the HY, the low temperatures registered in January 2017, which caused the stream to freeze, and the relatively high evapotranspiration during the summer period compared with the HY 2016/2017 (Figure 5). Accordingly, discharge was high for 8 months (from November 2015 to June 2016) during the HY 2015/2016 and only for 3 months (from February to

**TABLE 1** Characteristics of the investigated riparian areas

Rip. area	Area monitored with TIR imagery (m <sup>2</sup> )	Headwater reach	Riparian max width (m)	Perennial GW exfiltration observed	Area elevation (average—m.a.s.l.)	Group
L1	153.22	Yes	8.80	Yes	477	PSA
M1	83.80	No	5.86	No	479	N-PSpA
M2	168.95	No	10.37	Yes	480	PSpA
M3	231.69	Yes	9.53	Yes	483	PSA
R2	115.54	No	3.97	No	476	N-PSpA
R3	155.19	Yes	6.57	Yes	480	PSA
S2	169.66	No	8.87	Yes	464	PSpA

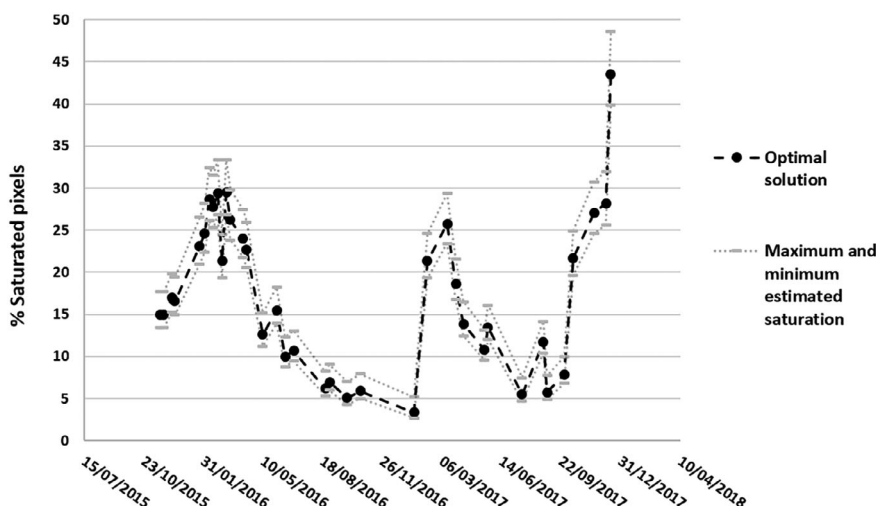


**FIGURE 7** Range of possible outcomes for the estimation of the percentage of saturated pixels for Area S2. Linear interpolations between the different observation dates are displayed as dotted and dashed lines and are meant to show the overall time series trend and might not reflect the actual saturation. The estimation for the other six investigated areas is reported in Figure A1



April 2017) during the HY 2016/2017. In December 2017, a rain-on-snow event produced a high peak discharge. Note that in January 2017, the stream was partially frozen (as a result, no discharge data are available for that period).

Shallow soil VWC (10-cm depth) gradually decreased from the riparian zone towards the hillslopes. Riparian soil VWC was oscillating between a maximum of ~70% during wet conditions and a minimum of ~65% during dry conditions. Shallow soil VWC at the other monitored locations was more variable (Figure 5), showing marked reaction to precipitation. Soil VWC of the shallow soil measured in

the Spruce-covered hillslope revealed a tendency of the soil to dry more rapidly than in other locations. Soil VWC measured in Sites 3 and 4 was generally more responsive to precipitation compared with soil VWC measured at Sites 5 and 7, at all depths (Figure 6). Soil VWC measured at Site 3 decreased from the 10-cm depth to the 60-cm depth, whereas the opposite was observed at Site 7. Soil VWC measured at Sites 4 and 5 was more similar along the depth profile (Figure 6). As previously observed, soil VWC profiles measured in the Spruce-covered and Pine-covered hillslopes at all depths revealed a tendency of the soil to dry more rapidly than in other locations. GW

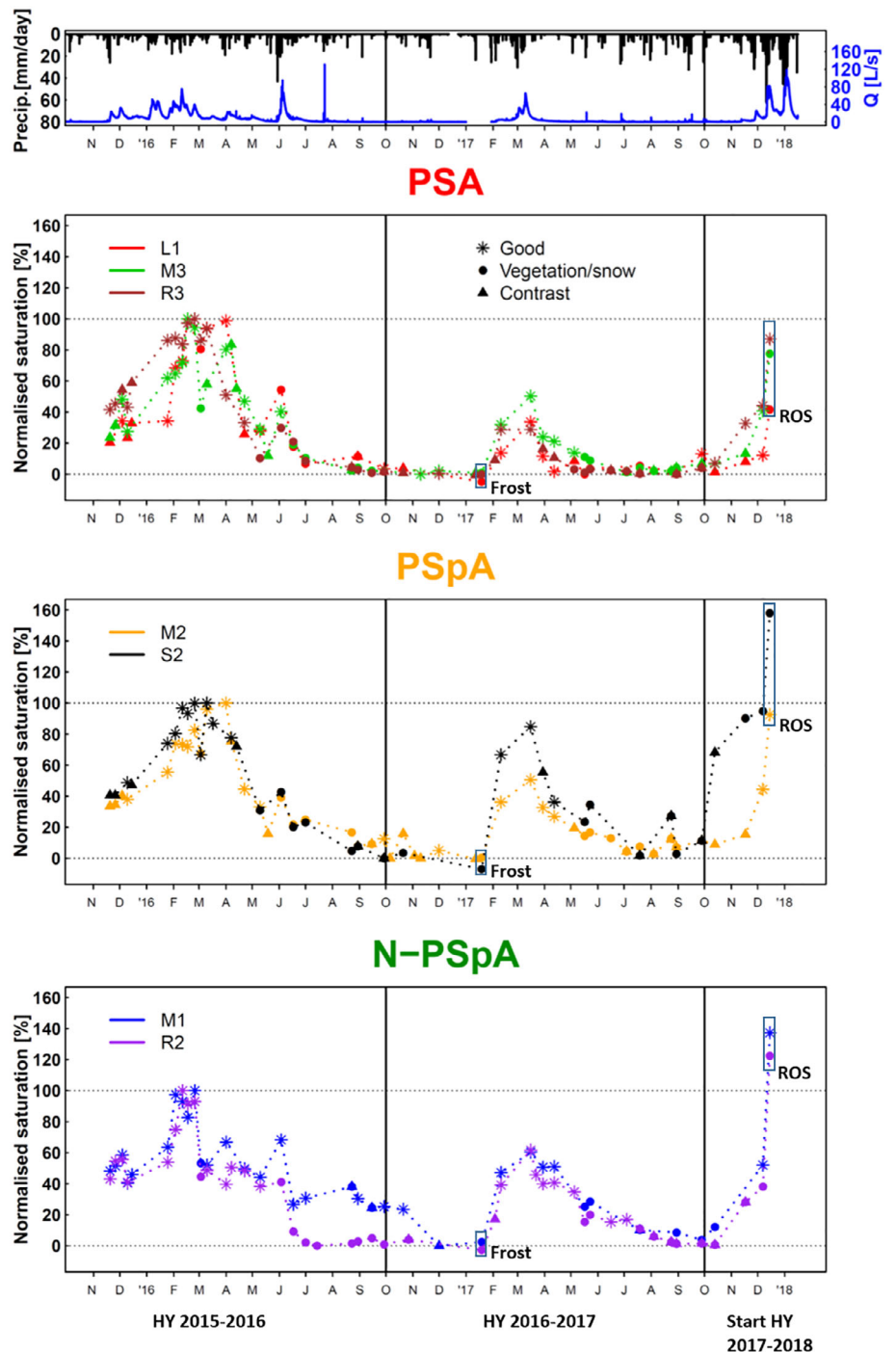


**FIGURE 8** Time series of precipitation and discharge (upper panel) and temporal evolution of normalized saturation obtained from thermal infrared (TIR) observations in the seven different riparian areas grouped according to the PSA, PSpA, and N-PSpA classification (PSA = Stream Source Areas with Perennial springs; PSpA = Areas along the stream with Perennial Springs; N-PSpA = Areas along the stream with Non-Perennial Springs). Out of the total number of 441 acquired TIR panoramas, 291 panoramas were used for the estimation of a value of surface saturation. Data represented with an asterisk refer to estimated values of surface saturation from TIR panoramas with optimal temperature contrast and no obstructive elements between the camera and the object ( $n = 101$ ). Data represented with a circle and a triangle refer to TIR observations that were slightly influenced by the presence of vegetation or snow ( $n = 110$ ) and where the temperature contrast was not optimal ( $n = 80$ ), respectively, but that were still usable for the estimation of a value of surface saturation. Normalization was done according to the highest and lowest observed percentage of saturation within each area individually, conditions with frost and rain-on-snow excluded. Frost = condition with frozen stream and riparian soil. ROS = rain-on-snow event

levels responded to precipitation in all four wells. Water levels in GW2 (close to a source area) and GW3 (hillslope foot) were always shallower than 2.00 m. GW5 and GW6 (both located on plateaus) behaved differently—mostly during dry periods, when the water level in GW5 would recede at a constant rate, whereas GW6 would dry quickly and show a reaction to new water inputs more similar to the response in soil moisture (also in comparison with the shallower GW2 and GW3).

During the wet periods, catchment storage and discharge showed very similar trends. During the dry periods—when catchment storage mainly corresponded to the GW reservoir—precipitation triggered more pronounced changes in discharge (as a single peak) in comparison with storage (cf. Figure 5b, red arrows).

## 4.2 | Characteristics of the investigated riparian areas and correspondent upslope catchments

We assigned the investigated riparian areas in the Weierbach catchment to three main groups, based on intrinsic area characteristics (Table 1). Areas L1, M3, and R3 correspond to the most upstream

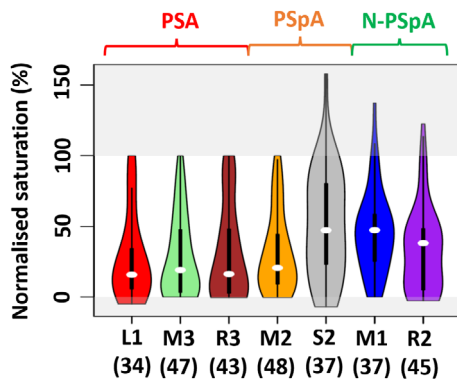


**FIGURE 9** Violin plots of the distribution of normalized surface saturation from the time series of the seven studied areas (grouped according to the PSA, PSpA, and N-PSpA classification: PSA = Stream Source Areas with Perennial springs; PSpA = Areas along the stream with Perennial Springs; N-PSpA = Areas along the stream with Non-Perennial Springs). Shaded areas highlight values of saturation acquired during particular boundary conditions such as frozen riparian soils (normalized saturation below 0%) and rain-on-snow events (normalized saturation above 100%). The number of samples used for each violin plot is indicated in brackets

Descriptive statistic	L1	M1	M2	M3	R2	R3	S2
Min	-4.90	0.00	-0.36	0.00	-2.74	-0.52	-6.98
Max	100.00	137.32	100.00	100.00	122.46	100.00	157.88
Mean	28.29	46.07	31.43	28.48	33.34	30.75	51.52
SD	30.60	29.80	28.51	28.93	30.15	33.49	38.06
Median	15.70	47.25	20.63	19.07	38.11	16.31	47.21

Note: L1,  $n = 34$ ; M1,  $n = 37$ ; M2,  $n = 48$ ; M3,  $n = 47$ ; R2,  $n = 45$ ; R3,  $n = 43$ ; S2,  $n = 37$ .  
Abbreviation: SD, standard deviation.

locations (i.e., source areas) of the stream. They are wide (8.3 m in average) and fed by perennial groundwater exfiltration (e.g., stable exfiltration points observed via TIR imagery throughout the year, cf. Figure 3). Areas M2 and S2 display similar characteristics but are located further downstream (Figure 3). In Areas M1 and R2, the riparian zones are narrower (4.9 m in average) and without clearly identified points of perennial groundwater exfiltration. On the basis of these differences, we qualify the first group as “Stream Source Areas with Perennial springs (PSA),” the second group as “Areas along the stream with Perennial Springs (PSpA),” and the third group as “Areas along the stream with Non-Perennial Springs (N-PSpA).”

## 4.3 | Range of surface saturation estimations

The estimated time series of surface saturation is shown with the range of maximum and minimum estimates of saturation for Area S2 as an example in Figure 7 (see Appendix A1 for the other areas). For all areas, the range between the calculated maximum and minimum estimates of saturation was larger (i.e., wider bounds around the optimal solution) for the panoramas presenting higher saturation and smaller (i.e., narrower bounds around the optimal solution) for the panoramas presenting lower saturation. Indeed, in TIR panoramas showing higher saturation, the threshold between the saturated and the unsaturated pixels often appeared less defined than in the TIR panorama showing lower saturation. The range between the maximum and minimum estimated saturation was narrow enough to preserve the general trend of the time series of estimated saturation as observed when considering the optimal solution. Thus, the temporal variability of surface saturation exceeded the variability that may derive from uncertain estimations of saturation (reflected in the range between the maximum and minimum estimates of saturation), and it is very likely that the overall estimated trend of saturation would remain similar, also if a different person would carry out the image processing procedure.

## 4.4 | Spatio-temporal dynamics of surface saturation and their relationship with meteorological conditions

The values of the estimated normalized surface saturation were highly monotonically related between the different areas over the whole

**TABLE 2** Summary of the descriptive statistics for the distribution of normalized surface saturation from the time series of the seven studied areas

study period (Spearman's rank test  $\rho$  not lower than 0.68 for all the correlations,  $p$  value  $< .01$ ). However, the seven areas reached their respective minima and maxima of saturation at different times (Figure 8). In January 2017, the occurrence of frozen water in the riparian area corresponded to very low surface saturation in all areas (i.e., normalized saturation below 0%), except for Areas M1 and M3, which reached their minimum saturation in December and November 2016, respectively. Maximum saturation in Areas M1, R2, and S2 resulted from a significant rain-on-snow event in December 2017 (i.e., normalized saturation above 100%). For the other four areas, the maximum level of saturation (i.e., normalized saturation = 100%) was reached in February 2016, under no particular meteorological conditions.

The distribution of normalized saturation from the time series was similar for Areas L1, M2, M3, R2, and R3 (Mann–Whitney–Wilcoxon test  $p$  value always higher than 0.05), whereas the distribution of Areas M1 and S2 was statistically different from all other areas (Mann–Whitney–Wilcoxon test  $p$  value always lower than 0.05 for

M1 and S2; Figure 9). Areas M1, R2, and S2 had particularly high median values (Figure 9; Table 2). The variability of the observations around the mean values (i.e., standard deviation) was similar for all areas (Table 2), although slightly higher in Area S2 (~38%). A summary of the descriptive statistics for the normalized saturation distribution of the seven riparian areas is reported in Table 2 and Figure 9. All areas presented a similar distribution of the daily rates of change in saturation (Mann–Whitney–Wilcoxon test  $p$  value always higher than .5, data not shown).

The comparison of the DMCs of rainfall–run-off and rainfall–surface saturation revealed a similar behaviour of run-off and surface saturation in all areas in response to precipitation and vegetative periods with high ET (Figure 10). From October to May of the HY 2015/2016, cumulated run-off and cumulated surface saturation consistently increased with increasing cumulated precipitation, whereas, with the beginning of the vegetative period in May (Figure 10—green shade), additional precipitation did not provoke an increase in cumulative run-off and surface saturation. Two events occurring in June and

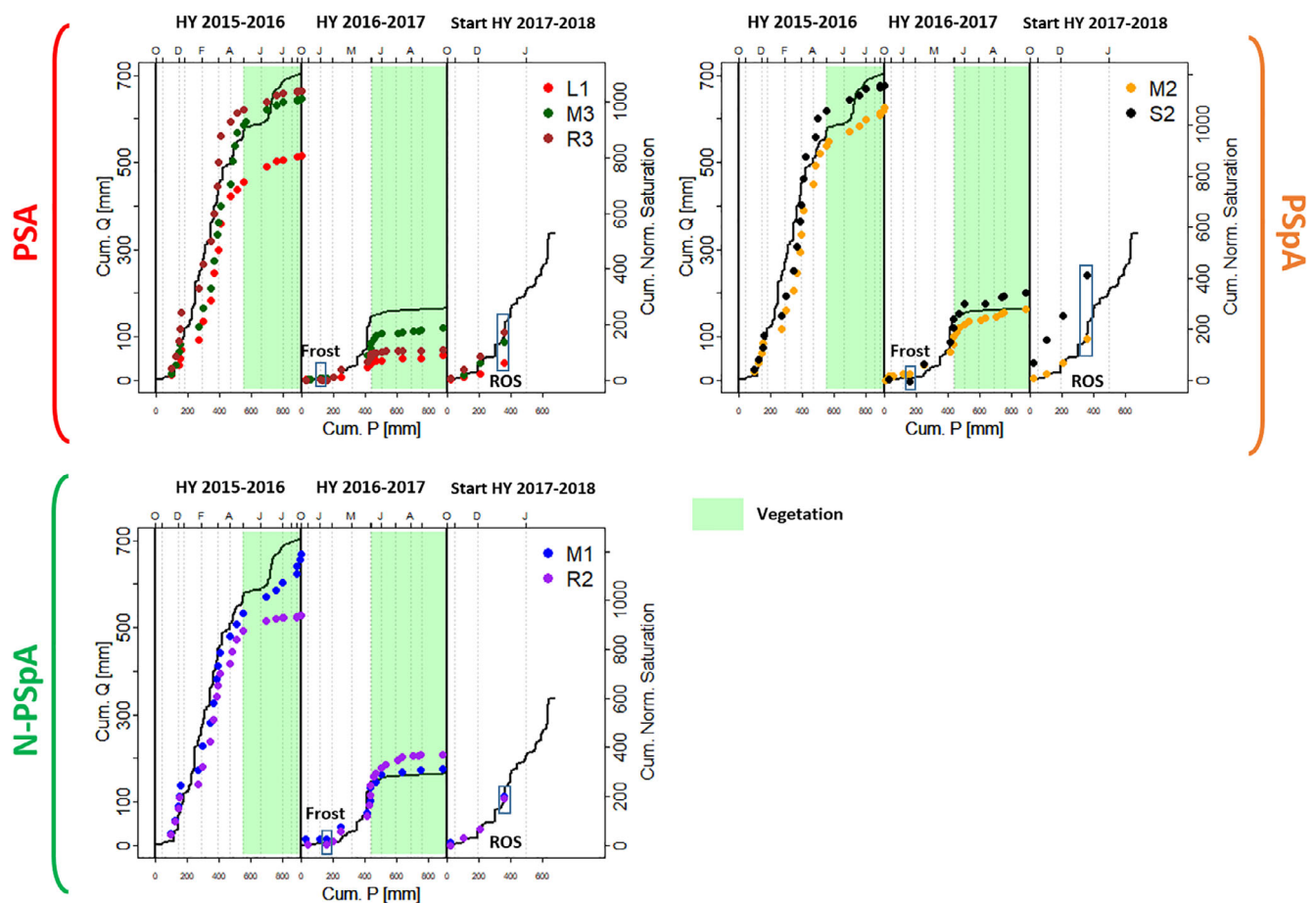


**FIGURE 10** Comparison between the rainfall–run-off double mass curves (DMCs; black line) and the surface saturation–run-off DMCs (coloured points) for the different investigated areas and hydrological years. Areas are grouped considering the PSA, PSpA, and N-PSpA classification (PSA = Stream Source Areas with Perennial springs; PSpA = Areas along the stream with Perennial Springs; N-PSpA = Areas along the stream with Non-Perennial Springs). Frost = condition with frozen stream and riparian soil. ROS = rain-on-snow event. Green shading = occurrence of vegetation, high estimated reference ET

July provoked cumulated run-off to sharply increase again, whereas cumulated surface saturation appeared to be affected by these events only in Areas M1 and M2. During the HY 2016/2017, both cumulative run-off and surface saturation remained low during a period of low precipitation amounts and low air temperatures with frost and started to accumulate with considerably higher amounts of

precipitation from February on. Cumulative run-off abruptly flattened with the beginning of the vegetative period while surface saturation flattened more gradually, especially in PSpA and Area R2. At the beginning of the HY 2017/2018, high precipitation and a rain-on-snow event caused both high cumulative amounts of run-off and surface saturation within a short period (especially in Area S2).

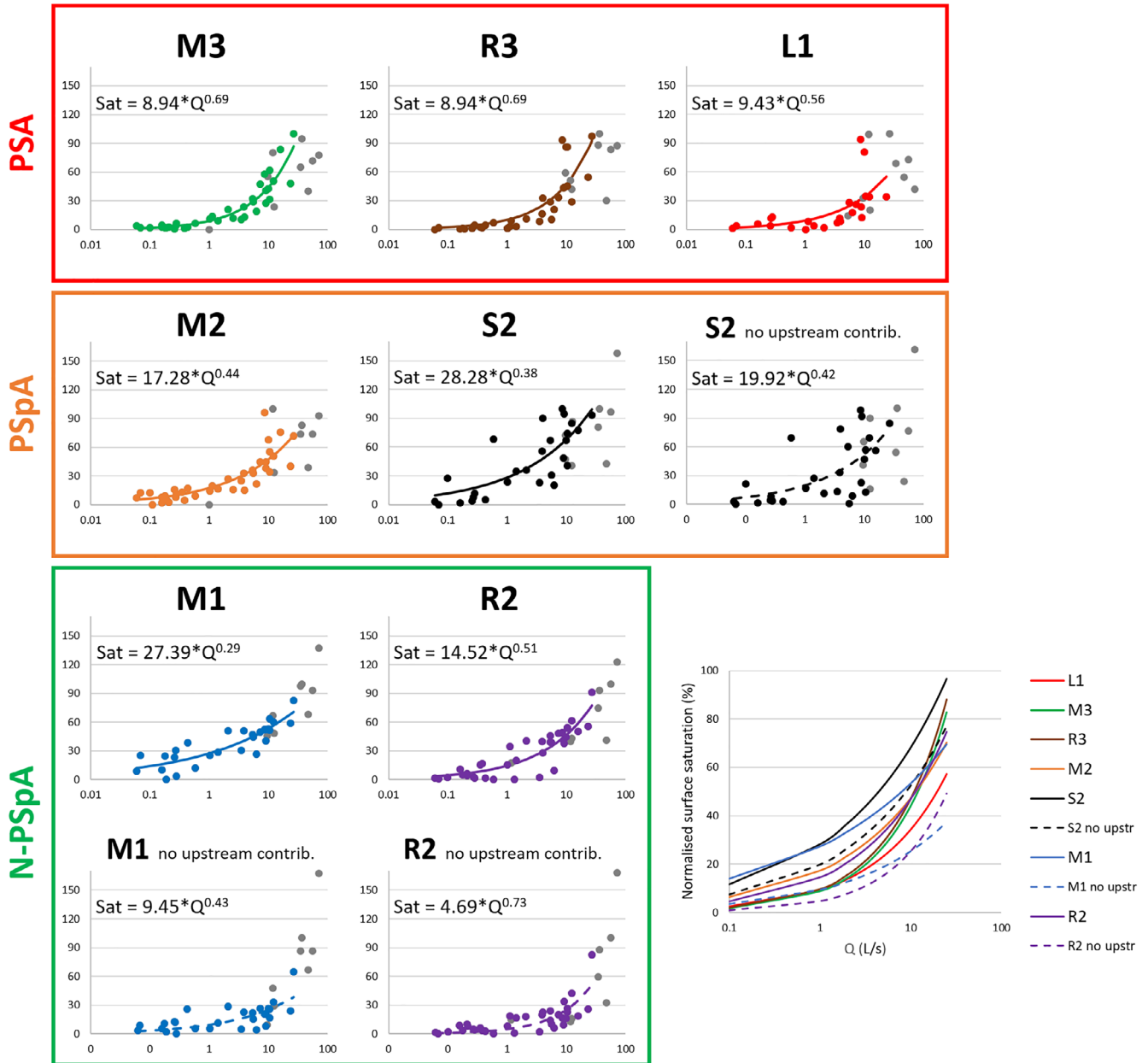


**FIGURE 11** Relationships between normalized saturation (Sat) and catchment baseflow discharge (Q) at the outlet (daily-averaged values) for the seven investigated riparian areas. Abscissa = normalized surface saturation (%); ordinate = discharge (L/s). The data are plotted with a logarithmic ordinate to visualize the relationships for low and high discharge values in details. Coloured dots represent the observations not impacted by the occurrence of precipitation (cf. Section 3.3). Grey dots represent observations influenced by precipitation during thermal infrared image acquisition. Continuous and dashed lines represent the power law relationships  $Sat = a \cdot Q^b$  fitted to the observations not impacted by the occurrence of precipitation (coloured dots only, nontransformed data). Plots marked with the wording “no upstream contribution” and dashed lines refer to the surface saturation data as estimated after having excluded the stream pixels from the images (cf. Section 3.2). Areas are grouped considering the PSA, PSpA and N-PSpA classification (PSA = Stream Source Areas with Perennial springs; PSpA = Areas along the stream with Perennial Springs; N-PSpA = Areas along the stream with Non-Perennial Springs)

#### 4.5 | Relationship between surface saturation dynamics and hydrometric measurements

For all riparian areas, we identified a strong monotonic relationship between normalized saturation and catchment discharge (Spearman's rank test  $\rho$  not lower than 0.78 for all areas,  $p$  value  $< .01$ ; Table 3). We found overall positive and significant monotonic relationships between the normalized saturation in the different areas and GW levels, VWC, and the estimated storage of the catchment (Table 3). In particular, estimated catchment storage showed higher correlation with normalized saturation in Areas M1, M2, and M3 ( $\rho \sim 0.92$ ). GW levels measured in Locations 2, 3, and 5 had in general higher correlation with normalized saturation ( $0.73 \leq \rho \leq 0.94$ ) compared with GW6 ( $0.59 \leq \rho \leq 0.75$ ) for all the areas. Soil VWC along the HRS transect had in general high correlation with normalized saturation in all areas ( $0.64 \leq \rho \leq 0.88$ ), with the lower correlation being between saturation in Area S2 and VWC measured at middle and foot hillslope positions and between saturation in Area L1 and VWC measured at riparian position. Soil VWC measured in Sites 3, 4, 5, and 7 at 10-, 20-, 40-, and 60-cm depth also was highly correlated with normalized surface saturation in all areas ( $0.67 \leq \rho \leq 0.88$ ), with the lower correlation being between saturation in Area S2 and VWC in all sites and depths. Also, VWC measured at Site 4 (low hillslope Spruce covered) was generally less correlated with normalized surface saturation in all investigated riparian areas.

Changes in the extent of surface saturation between two observation dates were significantly related to the changes of GW level in Location GW3 ( $0.60 < \rho < 0.77$ ). All the areas except Areas M2 and R2 showed also significant correlation with changes of GW level in GW2 ( $0.58 < \rho < 0.67$ ; Table 4). Area M1 was particularly correlated also with the GW levels measured in Location GW5 ( $\rho = 0.72$ ). Changes in the extent of surface saturation between two observation dates were also significantly related to the changes in catchment storage ( $0.65 < \rho < 0.84$ ) in all areas. A low but significant correlation of the changes of surface saturation with the antecedent precipitation index was observed for the Areas L1, M1, R2, and S2 ( $\rho = 0.50$ ). Changes in soil VWC along the HRS transect (10-cm depth) were not significantly correlated to changes in surface saturation between two observation dates for any of the investigated riparian areas (Table 4). Changes in soil VWC measured at Sites 3, 4, 5, and 7 at 10-, 20-, 40-, and 60-cm depth were significantly correlated to changes in surface saturation (except for Area L1 and soil VWC at Site 3 at 10-cm depth; Table 4). However, only surface saturation changes in Areas R3 and S2 showed a good correlation with changes in soil VWC measured at different sites and depths. In particular, surface saturation changes in Areas R3 and S2 were particularly related to changes in soil VWC measured at Sites 4 and 5 (at low and middle slope positions, respectively) with  $\rho \geq 0.56$  for Area R3 and  $\rho \geq 0.60$  for Area S2.

The surface saturation versus outlet baseflow discharge relationship has been investigated for the seven riparian areas (Figure 11). In Areas S2, M1, and R2, the observations obtained during low flow appeared more scattered than for the other areas, probably due to stream water contribution from upstream. In order to give an example

**TABLE 3** Spearman's rank correlation between the normalized saturation in the seven areas and hydrometric variables

Hydrometric variable	L1	M1	M2	M3	R2	R3	S2
Q	0.86	0.92	0.89	0.91	0.88	0.91	0.78
Stor_tot	0.84	0.93	0.92	0.91	0.87	0.89	0.74
GW2	0.83	0.90	0.89	0.91	0.87	0.91	0.79
GW3	0.86	0.89	0.88	0.90	0.85	0.94	0.84
GW5	0.82	0.92	0.91	0.91	0.84	0.85	0.73
GW6	0.59	0.66	0.71	0.74	0.69	0.75	0.69
VWC_U	0.80	0.83	0.87	0.88	0.78	0.86	0.71
VWC_M	0.79	0.80	0.85	0.86	0.76	0.82	0.64
VWC_F	0.79	0.83	0.85	0.87	0.76	0.78	0.69
VWC_R	0.65	0.83	0.86	0.85	0.70	0.77	0.75
VWC_S	0.83	0.76	0.78	0.79	0.70	0.82	0.67
Site 3 10 cm	0.84	0.82	0.86	0.88	0.79	0.86	0.71
Site 3 20 cm	0.80	0.81	0.82	0.83	0.79	0.83	0.70
Site 3 40 cm	0.84	0.84	0.85	0.87	0.81	0.87	0.73
Site 3 60 cm	0.82	0.82	0.84	0.85	0.8	0.85	0.71
Site 4 10 cm	0.82	0.78	0.76	0.77	0.72	0.81	0.67
Site 4 20 cm	0.79	0.79	0.75	0.75	0.72	0.79	0.70
Site 4 40 cm	0.82	0.79	0.76	0.76	0.72	0.80	0.69
Site 4 60 cm	0.81	0.79	0.76	0.76	0.72	0.80	0.69
Site 5 10 cm	0.84	0.81	0.81	0.84	0.75	0.84	0.78
Site 5 20 cm	0.84	0.82	0.80	0.83	0.75	0.84	0.75
Site 5 40 cm	0.83	0.84	0.81	0.84	0.76	0.86	0.76
Site 5 60 cm	0.83	0.83	0.81	0.83	0.75	0.84	0.76
Site 7 10 cm	0.83	0.80	0.84	0.86	0.79	0.84	0.68
Site 7 20 cm	0.83	0.81	0.83	0.86	0.80	0.85	0.70
Site 7 40 cm	0.80	0.79	0.82	0.84	0.77	0.82	0.67
Site 7 60 cm	0.79	0.82	0.85	0.88	0.81	0.86	0.71

Note: All shown correlations are significant with  $\alpha = .01$ . Q = catchment discharge (l/s) at catchment outlet; Stor\_tot = total catchment storage; GW = ground water; VWC\_U = volumetric water content (VWC) in upslope position (beech covered); VWC\_M = VWC in middle slope position; VWC\_F = VWC in foot of the slope position; VWC\_R = VWC in riparian zone; VWC\_S = VWC in upslope position (spruce covered). Site 3 10 cm = VWC measured at Site 3 at 10-cm depth (similar naming for the other VWC sites and depths).

of a reduced influence of upstream water contribution in Areas M1, R2, and S2, we re-estimated the extent of surface saturation after having excluded stream pixels from the TIR images. One can notice a general shift towards lower saturation for Areas M1 and R2 (see Figure 11, M1, R2, and S2 "no upstream contr."). This is less pronounced for Area S2, probably as a result of the presence of permanent springs within this area, which maintain the riparian zone generally wetter. In general, scattering in the observations at low flow appears reduced in Areas S2, M1, and R2 after having reduced the influence of upstream water contribution. Note that we did not apply the exercise of reducing upstream contribution to Area M2, because we frequently inferred from the TIR images that the portion of stream



**TABLE 4** Spearman's rank correlation between the changes in the amount of surface saturation between two consecutive observation dates and changes of hydrometric variables (GW = ground water; Stor\_tot = total catchment storage; Site 3 10 cm = soil volumetric water content measured at Site 3 at 10-cm depth—similar naming for the other sites and depths) and antecedent precipitation index (API) calculated between the same observation dates

Hydrometric variable	L1	M1	M2	M3	R2	R3	S2
GW2	0.58	0.67	0.50	0.62	0.65	0.55	0.60
GW3	0.60	0.62	0.59	0.65	0.77	0.71	0.76
GW5	0.50	0.72	0.45	0.54	0.57	0.47	0.54
GW6	0.36	0.42	0.42	0.47	0.63	0.57	0.61
API	0.51	0.53	0.48	0.42	0.50	0.35	0.50
Stor_tot	0.66	0.84	0.65	0.71	0.66	0.67	0.68
Site 3 10 cm	/	0.46	0.38	0.38	0.34	0.49	0.57
Site 3 20 cm	/	0.42	0.41	0.36	0.33	0.48	0.54
Site 3 40 cm	/	0.45	0.40	0.37	0.34	0.48	0.55
Site 3 60 cm	/	0.43	0.40	0.36	0.34	0.48	0.54
Site 4 10 cm	0.37	0.45	0.47	0.46	0.35	0.59	0.62
Site 4 20 cm	0.38	0.50	0.45	0.43	0.39	0.56	0.66
Site 4 40 cm	0.40	0.47	0.46	0.46	0.38	0.59	0.64
Site 4 60 cm	0.39	0.50	0.45	0.44	0.38	0.57	0.64
Site 5 10 cm	0.38	0.47	0.52	0.53	0.42	0.70	0.60
Site 5 20 cm	0.39	0.47	0.51	0.51	0.42	0.67	0.60
Site 5 40 cm	0.39	0.46	0.41	0.51	0.45	0.66	0.61
Site 5 60 cm	0.38	0.46	0.46	0.50	0.43	0.66	0.61
Site 7 10 cm	0.28	0.44	0.36	0.36	0.32	0.45	0.56
Site 7 20 cm	0.25	0.40	0.37	0.35	0.31	0.46	0.53
Site 7 40 cm	0.27	0.40	0.36	0.34	0.29	0.46	0.51
Site 7 60 cm	0.27	0.44	0.42	0.37	0.29	0.51	0.55

Note: All shown correlations are significant with  $\alpha = .01$ . Changes in soil volumetric water content measured at 10-cm depth along the hillslope-riparian-stream transect did not show significant correlation with changes in surface saturation.

before the perennial riparian inflow in Area M2 was dry. Analysing the fitted curves for the surface saturation versus baseflow discharge relationship for PSpA and N-PSpA (see Figure 11), saturation in PSpA had an overall similar relationship with baseflow discharge: Saturation in the two areas increased with higher discharge following a similar power law, especially when considering the saturation in Area S2 after the effect of the upstream contribution has been attenuated. The N-PSpA saturation versus baseflow discharge relationship seemed to differ between each other and from the other areas, both before and after reducing the effect of upstream contributions. Finally, surface saturation in PSA presented similar relationships with baseflow discharge during low discharge rates. However, as baseflow discharge increased, saturation in Areas M3 and R3 increased faster compared with Area L1 and the other areas in general. When considering the observations affected by precipitation (Figure 11, grey dots), a slight hysteretic effect could be observed for the surface saturation versus

discharge relationship, in particular for Areas L1, M2, M3, and R3 at higher discharge.

## 5 | DISCUSSION

We have used ground-based TIR imagery for mapping the spatio-temporal dynamics of riparian surface saturation expansion and contraction in the Weierbach catchment. For the first time, the dynamics of surface saturation in different riparian locations within the same catchment have been monitored at a temporal resolution high enough to characterize their seasonal variability. To the best of our knowledge, prior to this study, extensive time series of surface saturation dynamics have been displayed only as model outputs, often considering the overall amount of saturation in the catchment and rarely being validated (Birkel et al., 2010; Weill et al., 2013). We observed strong similarity in the expansion/contraction dynamics between the seven riparian surface saturated areas over the whole study period, although there were some differences in the timing of maximum or minimum levels of saturation in the seven areas. N-PSpA and Area S2 showed generally higher normalized surface saturation values (i.e., high median value). The maximum of surface saturation in these areas occurred during a rain-on-snow event in December 2017. This is likely due to the fact that these areas receive the highest contributions of stream water from upstream than other areas (i.e., Area M2 and PSA; cf. areas' locations in Figure 3). We observed the lowest surface saturation extensions between November 2016 and January 2017 in all areas. For most of them, the lowest saturation values corresponded to the occurrence of frozen water in the riparian zone. On these occasions, the low values of surface saturation are likely to be the result of the combination of a dry period (i.e., lower amount of GW exfiltration and less water in the stream channel) and the fact that surface water in the riparian zone was frozen. We did not consider frozen surface water in the riparian zone as being surface saturation, because frozen (solid) water exhibits different characteristics than free (liquid) water, for example, in terms of reaction to incident precipitation or movement dynamics.

The yearly and seasonal variability in the dynamics of surface saturation in the seven areas was found to reflect the yearly and seasonal variability of catchment run-off (cf. Figures 8 and 10). Increasing cumulated amounts of precipitation caused cumulated run-off and surface saturation to increase in a similar way during the wet periods. Increasing ET losses during the vegetative period led to moments of low run-off and low surface saturation (i.e., flatter cumulated run-off and surface saturation) despite that the amount of precipitation did not change considerably. Occurrence of breaks along the DMCs when passing from wet to dry conditions—and vice versa—were very similar between the rainfall-run-off and the rainfall-surface saturation DMCs. However, breaks and slope changes in the rainfall-surface saturation DMCs were generally less sharp than the slope changes observed in the rainfall-run-off DMCs. Martínez-Carreras et al. (2016) showed that the Weierbach catchment's run-off response is influenced by a storage threshold that, once exceeded, allows high



discharge volumes to be generated by the catchment even in response to relatively small precipitation events. The similarity between the break points in the run-off and surface saturation DMCs may indicate that the same storage threshold influences the seasonal transition between low and high extents of surface saturation in the riparian areas. However, other aspects may play a role in regulating the seasonal expansion and contraction of surface saturation as well. For example, the smoother slope changes in the surface saturation DMCs than run-off DMCs may reflect that riparian soil hydraulic characteristics influence the expansion and contraction of surface saturation by defining the degree of resilience of surface saturation to develop in response to increasing and decreasing catchment's wetness conditions. In this sense, the seasonal transition of riparian surface saturation may be subjected to a second, different threshold, which is defined by the riparian soil capacity to store and release water (Zehe, Lee, & Sivapalan, 2006). In order to further investigate the presence of thresholds for the development of surface saturation, a more frequent mapping during the seasonal transitions (i.e., by installing TIR fixed cameras) would have been required and might be targeted for the future.

Overall, the dynamics of saturation in the seven areas reflected the hydrological response of the catchment observed in terms of discharge, GW, soil VWC, and estimated catchment storage (high Spearman's rank correlation between normalized surface saturation and discharge, GW, soil VWC, and estimated catchment storage). Moreover, the daily-normalized rates at which surface saturation changed (i.e., increasing or decreasing) between the different observation dates were similar for all areas. These results indicate that the different areas in the riparian zone reacted to changes in the wetness state of the catchment in a similar way. Similarities between the different riparian areas emerged also from the comparison of the changes in surface saturation between two consecutive dates with the changes of the other hydrometric measurements between the same two consecutive dates (Table 4). Changes in surface saturation were particularly related to changes in catchment storage for all the investigated areas. Moreover, changes in surface saturation in the riparian areas were well related to changes in GW levels recorded at the hillslope foot position (GW3) and close to the riparian zone (GW2) for all investigated areas, except for Area M1. The good relationship between both changes in catchment storage and GW levels recorded in GW3 and changes in surface saturation may suggest that the saturated compartment of the catchment storage ( $S_{SAT}$ ) and, specifically, the hillslope GW storage (estimated from GW3) may be the storage compartment relating the most with the riparian surface saturation dynamics observed in the different areas.

Water table variations observed in GW3 and GW2 are indicative for GW fluctuations within the *solum* and *subsolum* layers in the Weierbach catchment (*solum* and *subsolum* layers profile observed from soil pits and cores—Moragues-Quiroga et al., 2017). These layers have been shown to play a significant role in the establishment of lateral GW connectivity between the hillslopes and the stream in the Weierbach catchment, especially during wet conditions (Martínez-Carreras et al., 2016; Rodríguez & Klaus, 2019; Wrede et al., 2014).

Similarly, our findings suggest that fluxes of GW from these layers may substantially contribute to sustaining riparian surface saturation during wet conditions in all investigated areas. Additionally, observed perennial GW exfiltration points (cf. Figure 3, red circles) supported surface saturation in PSA and PSpA during both wet and dry conditions. Our observations are consistent with studies from other catchments that have assessed the role of GW level fluctuations occurring at middle and low hillslope locations in controlling the connectivity between the hillslopes and the riparian zone. In example, McGlynn and McDonnell (2003) found that the expansion of the saturated area was consistent with GW level dynamics in the lower hillslope and hollow zones in the Maimai catchment. Van Meerveld, Seibert, and Peters (2015) noted in the Panola catchment that the hillslope and the riparian zone only became connected when GW levels rose in the lower part of the hillslope.

We did not observe a consistent relationship between changes in surface saturation and changes in soil VWC measured at different soil profiles. However, changes in surface saturation in Areas R3 and S2 showed good correlation with changes in soil VWC measured in Sites 4 (low hillslope) and 5 (midhillslope) at all depths (Table 4). Although this result may suggest that variability in the unsaturated compartment of the catchment storage ( $S_{UNSAT}$ —estimated from the VWC of the soil profiles) could be related with the dynamics of riparian surface saturation in some areas, this particular relationship remains of difficult interpretation, and further investigation on the water sources of riparian surface saturation is currently ongoing.

Considering the observed seasonal dynamics of surface saturation and the possible influence of lower hillslope GW fluctuations on surface saturation, we provide a perceptual model of how riparian surface saturation may evolve in the different monitored areas in Weierbach catchment during dry and wet periods, in the absence of precipitation (Figure 12). Note that our perceptual model is based on a combination of the visual inspection of the TIR observations (i.e., the presence of perennial GW exfiltration and surface saturation patterns), estimated surface saturation time series, and statistical correlations. Future investigations employing tracers, additional GW level measurements, or modelling might be useful to further refine and corroborate our perceptual model. On the basis of our current knowledge, we assume that the observed dynamics of surface saturation are the result of an interplay between the wetness state of the catchment and the morphological features of the observed areas (i.e., area width and elevation and existence of GW exfiltration points). During the dry season, perennial groundwater exfiltration supports the saturation in PSA and Area M2 (Figure 12a). In N-PSpA, saturation (when present) is mainly represented by water in the stream channel. We assume this water to be mainly the result of upstream contributions (cf. Figure 12d, discussion of longitudinal/upstream contribution in Section 3.2) because no perennial groundwater exfiltration points were detected in these areas during dry conditions. Moreover, some groundwater may exfiltrate directly into the stream channel from the hyporheic zone. Especially in Area M1, saturation during the dry season was observed to be quite high, likely because this area receives contributions from two upstream areas with perennial groundwater

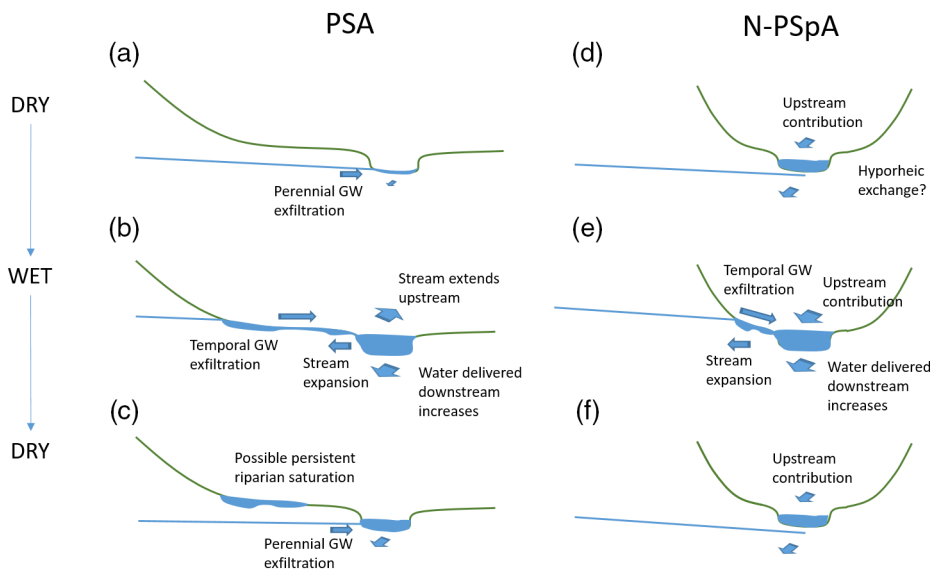


**FIGURE 12** Proposed perceptual model for the development of surface saturation in PSA (Stream Source Areas with Perennial springs) and N-PSPA (Areas along the stream with Non-Perennial Springs) riparian areas

exfiltration, that is, Areas M2 and M3. Similarly, Area S2 could exhibit high saturation because both perennial groundwater exfiltration and upstream contributions are present. During the wet season, as groundwater levels increase, saturation in PSA and PSpA develops extensively as riparian saturation and in the previously dry stream bed upstream (Figure 12b). Saturation in N-PSPA is assumed to increase during the wet season mainly due to higher contribution from upstream and from temporary springs that activate in the riparian zone (especially in Area M1; Figure 12e). In addition, the extension of surface saturation in the different areas may be influenced by stream expansion into the riparian zone (cf. Glaser et al., 2018; Figure 12b,e). When passing again from wet to dry conditions, PSA and PSpA showed more persistent surface saturation in the riparian zone compared with N-PSPA (observed from TIR observations). This may be related to the fact that PSA and PSpA are generally wider than N-PSPA and can produce more extensive surface saturation, which seems to dry slower (Glaser, Antonelli, Hopp, & Klaus, 2019; Figure 12c,f). We hypothesize that the presence of perennial springs in PSA and PSpA may contribute to keep the area generally wetter during the drying down period. At the occurrence of precipitation and events like rain-on-snow, surface saturation development can be the result of the processes illustrated in Figure 12 combined with the occurrence of infiltration excess.

The saturation–baseflow discharge relationships observed in the different riparian areas can be related to the dynamics illustrated in the perceptual model in Figure 12. At low flow, the differences observed in the saturation–baseflow discharge relationships (i.e., amount of surface saturation and scattering in the observations, cf. Figure 11) can be explained by the presence of perennial springs and the location of the riparian area (i.e., area elevation—which determines the variable amount of water reaching the area from upstream locations). At higher flow, the possibility for saturation to develop upstream in PSA (cf. Figure 12b) could explain the fast change in saturation with increasing baseflow discharge in these areas compared with the others (cf. Figure 11). Indeed, it also has been observed by

others that saturation that develops in previously dry channels is more reactive than saturation in riparian areas, which is rather influenced by the speed at which the soil drains (Dunne et al., 1975). The development of more persistent saturation in the riparian soils than the stream channel (Figure 12c) may explain the slight hysteretic effect that was observed in the saturation–discharge relationship of PSA and Area M2 (cf. Figure 11—grey dots). The hysteretic relationships between saturation and discharge that we observed in some areas provide a first actual feedback to the possible hysteretic relationship between surface saturation and outlet discharge that has been usually observed through modelling approach (Glaser et al., 2016; Weill et al., 2013). However, the hysteretic relationships between saturation and discharge observed in this study were never as clearly defined as those observed in modelling studies (Frei et al., 2010; Weill et al., 2013), despite the relatively high number of observations at high flow stages. In this sense, TIR observations at a higher temporal resolution during precipitation events would help to clarify the hysteretic patterns that may occur in the different areas and could be used to validate hysteretic behaviour observed through simulations. Overall, the small but noticeable differences observed in the saturation–baseflow discharge relationships provided information on the different potential for lateral and longitudinal hydrological connectivity to be established through the different riparian areas during different flow stages.

To date, surface saturation–baseflow discharge relationships have been inferred considering only the total surface saturation extent in a catchment (Ambroise, 2016; Latron & Gallart, 2007). The surface saturation–baseflow discharge relationship has been defined by Ambroise (2016) as a characteristic curve of the catchment, fundamental for understanding and modelling the interaction of water from different sources on the saturated areas and its influence on streamflow during baseflow conditions. By repeatedly monitoring the dynamics of surface saturation in different areas, we found indication of possible intracatchment variability of this relationship. Moreover, the frequency at which we observed surface saturation in this study

allowed us to explore the dynamics of surface saturation during baseflow conditions under different flow stages. It also allowed us to consider how seasonality may affect the observed dynamics. Considering the fact that the broadly used topography-driven indices and geomorphic indices for estimating surface saturation are known to perform relatively poorly during low flow stages (Ali et al., 2013; Güntner, Seibert, & Uhlenbrook, 2004; Western, Grayson, Blöschl, Willgoose, & McMahon, 1999), our observation of surface saturation dynamics during low baseflow conditions is particularly valuable for obtaining new insights into riparian processes and potentially improve these indices. In example, from the analysis of the rainfall–surface saturation DMCs, we observed that increasing ET losses during the vegetative period lead to moments of low surface saturation despite the amount of precipitation did not change considerably. The neglect of this shift in dominant processes in the indices calculation might be the reason for the poor performance during dry periods.

## 6 | CONCLUSIONS

This study is a contribution to the call for the development of a routine method for mapping surface saturated areas (Dunne et al., 1975) and to the need to start characterizing the spatial and temporal variability of riparian processes for a better understanding of catchments hydrological and biochemical functioning (Grabs et al., 2012; Ledesma et al., 2018; Tetzlaff et al., 2008; Vidon & Hill, 2004). We applied TIR technology as a valid routine method for repeated mapping of surface saturation (in our case, at weekly or biweekly frequency) in the Weierbach catchment. The frequency at which we monitored surface saturation was critical to characterize the similarities and differences in both the temporal dynamics of surface saturation in different areas and their relationship with stream baseflow discharge.

The observed yearly and seasonal dynamics of surface saturation in the different riparian areas of the catchment were found to be similar. Based on the analysis of DMCs for the surface saturation in comparison with the DMC of discharge, we hypothesized that storage thresholds control the transition between low extents of surface saturation and high extents of surface saturation in the Weierbach catchment. Another similarity between the dynamics of surface saturation observed in different investigated areas has been found in their relationship with the variability in catchment's storage and GW levels measured in lower hillslope locations. This supports the role of riparian surface saturation as a valuable indicator of groundwater storage during baseflow conditions previously assessed in different studies (i.e., Ambrose, 2016; Gburek & Sharpley, 1998; Myrabø, 1997).

The shape of the relationship between surface saturation and baseflow discharge could be approximated with a power law in all cases. However, small differences in the relationships for the different areas could be associated with the location of the areas along the stream network (i.e., area elevation) and with the local riparian morphology (i.e., area width and the presence of GW exfiltration points).

These characteristics represent a source of intracatchment variability that may have implications on the potential of different riparian surface saturated areas in mediating hydrological connectivity along the HRS continuum.

Based on our findings and conclusions, we may now ask “Are all riparian zones in our catchment the same, or would the small differences in their dynamics of surface saturation mirror the degree of hydrological connectivity of the different areas with the hillslopes?” With this question in mind, we will present our investigation on the spatial heterogeneity of streamflow generation in our second contribution. The data and information obtained in this study will prove essential for investigating the spatial variability of streamflow generation in the Weierbach catchment and its relationship with surface saturation. The same approach used in this study can be potentially employed in other catchments as well, especially in those where the riparian zone represents an important interface between the hillslopes and the stream.

## ACKNOWLEDGMENTS

We would like to thank Jean-Francois Iffly, the Observatory for Climate and Environment of the Luxembourg Institute of Science and Technology, and the Administration des Services Techniques de l'Agriculture (ASTA) for the collection and provision of the hydrometrical and meteorological data. We would like to thank Núria Martínez-Carreras for the estimation of catchment storage. Marta Antonelli was funded by the European Union's Seventh Framework Programme for research, technological development, and demonstration under Grant agreement no. 607150 (FP7-PEOPLE-2013-ITN—INTERFACES—Ecohydrological interfaces as critical hotspots for transformation of ecosystem exchange fluxes and biogeochemical cycling). Barbara Glaser was funded by the Luxembourg National Research Fund (FNR) FNR35 AFR Pathfinder project (ID 10189601).

## CONFLICT OF INTEREST

The authors declare that they have no conflict of interest.

## DATA AVAILABILITY STATEMENT

Data used in this study are property of the Luxembourg Institute of Science and Technology. They are available upon request from the authors.

## ORCID

Marta Antonelli  <https://orcid.org/0000-0001-9560-1981>

Laurent Pfister  <https://orcid.org/0000-0001-5494-5753>

## REFERENCES

- Ali, G., Birkel, C., Tetzlaff, D., Soulsby, C., McDonnell, J. J., & Tarolli, P. (2013). A comparison of wetness indices for the prediction of observed connected saturated areas under contrasting conditions. *Earth Surface Processes and Landforms*, 39(3), 399–413. <https://doi.org/10.1002/esp.3506>
- Allen, R. G., Pereira, L. S., Raes, D., Smith, M., & Ab, W. (1998). Crop evapotranspiration—Guidelines for computing crop water requirements. *Irrigation and Drainage Paper No. 56*, FAO, 300. <https://doi.org/10.1016/j.eja.2010.12.001>

- de Alwis, D. A., Easton, Z. M., Dahlke, H. E., Philpot, W. D., & Steenhuis, T. S. (2007). Unsupervised classification of saturated areas using a time series of remotely sensed images. *Hydrology and Earth System Sciences*, 11(5), 1609–1620. <https://doi.org/10.5194/hess-11-1609-2007>
- Ambrose, B. (2004). Variable 'active' versus 'contributing' areas or periods: A necessary distinction. *Hydrological Processes*, 18(6), 1149–1155. <https://doi.org/10.1002/hyp.5536>
- Ambrose, B. (2016). Variable water-saturated areas and streamflow generation in the small Ringelbach catchment (Vosges Mountains, France): The master recession curve as an equilibrium curve for interactions between atmosphere, surface and ground waters. *Hydrological Processes*, 30(20), 3560–3577. <https://doi.org/10.1002/hyp.10947>
- Appels, W. M., Bogaart, P. W., & van der Zee, S. E. A. T. M. (2016). Surface runoff in flat terrain: How field topography and runoff generating processes control hydrological connectivity. *Journal of Hydrology*, 534, 493–504. <https://doi.org/10.1016/j.jhydrol.2016.01.021>
- Baker, M. E., Wiley, M. J., & Seelbach, P. W. (2001). GIS-based hydrologic modeling of riparian areas: Implications for stream water quality. *Journal of the American Water Resources Association*, 37(6), 1615–1628.
- Beven, K. J., & Kirkby, M. J. (1979). A physically based, variable contributing area model of basin hydrology. *Hydrological Sciences Bulletin*, 24(1), 43–69. <https://doi.org/10.1080/02626667909491834>
- Birkel, C., Tetzlaff, D., Dunn, S. M., & Soulsby, C. (2010). Towards a simple dynamic process conceptualization in rainfall-runoff models using multi-criteria calibration and tracers in temperate, upland catchments. *Hydrological Processes*, 24, 260–275. <https://doi.org/10.1002/hyp.7478>
- Blumstock, M., Tetzlaff, D., Dick, J. J., Nuetzmann, G., & Soulsby, C. (2016). Spatial organization of groundwater dynamics and streamflow response from different hydrogeological units in a montane catchment. *Hydrological Processes*, 30(21), 3735–3753. <https://doi.org/10.1002/hyp.10848>
- Bracken, L. J., & Croke, J. (2007). The concept of hydrological connectivity and its contribution to understanding runoff-dominated geomorphic systems. *Hydrological Processes*, 21(13), 1749–1763. <https://doi.org/10.1002/hyp.6313>
- Briggs, M. A., Dawson, C. B., Holmquist-Johnson, C. L., Williams, K. H., & Lane, J. W. (2019). Efficient hydrogeological characterization of remote stream corridors using drones. *Hydrological Processes*, 33(2), 316–319. <https://doi.org/10.1002/hyp.13332>
- Coles, A. E., & McDonnell, J. J. (2018). Fill and spill drives runoff connectivity over frozen ground. *Journal of Hydrology*, 558, 115–128. <https://doi.org/10.1016/j.jhydrol.2018.01.016>
- Dick, J. J., Tetzlaff, D., Birkel, C., & Soulsby, C. (2015). Modelling landscape controls on dissolved organic carbon sources and fluxes to streams. *Biogeochemistry*, 122(2–3), 361–374. <https://doi.org/10.1007/s10533-014-0046-3>
- Dunne, T., & Black, R. D. (1970). An experimental investigation of runoff production in permeable soils. *Water Resources Research*, 6(2), 478–490. <https://doi.org/10.1029/WR006i002p00478>
- Dunne, T., Moore, T. R., & Taylor, C. H. (1975). Recognition and prediction of runoff-producing zones in humid regions. *Hydrological Sciences Bulletin*, 20(3), 305–327. [https://doi.org/Cited By \(since 1996\) 102 \rExport Date April 4, 2012](https://doi.org/Cited%20By%20(since%201996)%20102%20Export%20Date%20April%204%202012)
- Fenicia, F., Kavetski, D., Savenije, H. H. G., Clark, M. P., Schoups, G., Pfister, L., & Freer, J. (2014). Catchment properties, function, and conceptual model representation: Is there a correspondence? *Hydrological Processes*, 28(4), 2451–2467. <https://doi.org/10.1002/hyp.9726>
- Frei, S., Lischeid, G., & Fleckenstein, J. H. (2010). Effects of micro-topography on surface-subsurface exchange and runoff generation in a virtual riparian wetland—A modeling study. *Advances in Water Resources*, 33(11), 1388–1401. <https://doi.org/10.1016/j.advwatres.2010.07.006>
- Gburek, W. J., & Sharpley, A. N. (1998). Hydrologic controls on phosphorus loss from upland agricultural watersheds. *Journal of Environment Quality*, 27(2), 267–277. <https://doi.org/10.2134/jeq1998.00472425002700020005x>
- Glaser, B., Antonelli, M., Chini, M., Pfister, L., & Klaus, J. (2018). Technical note: Mapping surface-saturation dynamics with thermal infrared imagery. *Hydrology and Earth System Sciences*, 22(11), 5987–6003. <https://doi.org/10.5194/hess-22-5987-2018>
- Glaser, B., Antonelli, M., Hopp, L., & Klaus, J. (2019). Intra-catchment variability of surface saturation—insights from long term observations and simulations. *Hydrology and Earth System Sciences Discussions*, 1–22. <https://doi.org/10.5194/hess-2019-203>
- Glaser, B., Klaus, J., Frei, S., Frentress, J., Pfister, L., & Hopp, L. (2016). On the value of surface saturated area dynamics mapped with thermal infrared imagery for modeling the hillslope-riparian-stream continuum. *Water Resources Research*, 52(10), 8317–8342. <https://doi.org/10.1002/2015WR018414>
- Gourdol, L., Clément, R., Juilleret, J., Pfister, L., & Hissler, C. (2018). Large-scale ERT surveys for investigating shallow regolith properties and architecture. *Hydrology and Earth System Sciences Discussions*, (December), 1–39. <https://doi.org/10.5194/hess-2018-519>
- Grabs, T., Bishop, K., Laudon, H., Lyon, S. W., & Seibert, J. (2012). Riparian zone hydrology and soil water total organic carbon (TOC): Implications for spatial variability and upscaling of lateral riparian TOC exports. *Biogeochemistry*, 9(10), 3901–3916. <https://doi.org/10.5194/bg-9-3901-2012>
- Grabs, T., Seibert, J., Bishop, K., & Laudon, H. (2009). Modeling spatial patterns of saturated areas: A comparison of the topographic wetness index and a dynamic distributed model. *Journal of Hydrology*, 373(1–2), 15–23. <https://doi.org/10.1016/j.jhydrol.2009.03.031>
- Güntner, A., Seibert, J., & Uhlenbrook, S. (2004). Modeling spatial patterns of saturated areas: An evaluation of different terrain indices. *Water Resources Research*, 40(5), 1–19. <https://doi.org/10.1029/2003WR002864>
- Hewlett, J. D. (1961). Soil moisture as a source of baseflow from steep mountain watersheds. *Southeastern Forest Experiment Station Asheville, North Carolina*, 132, 1–11.
- Juilleret, J., Iffly, J. F., Pfister, L., & Hissler, C. (2011). Remarkable Pleistocene periglacial slope deposits in Luxembourg (Oesling): Pedological implication and geosite potential. *Bulletin de La Société des Naturalistes Luxembourgeois*, 112(1), 125–130. Retrieved from [http://www.snl.lu/publications/bulletin/SNL\\_2011\\_112\\_125\\_130.pdf](http://www.snl.lu/publications/bulletin/SNL_2011_112_125_130.pdf)
- Klaus, J., Wetzel, C. E., Martínez-Carreras, N., Ector, L., & Pfister, L. (2015). A tracer to bridge the scales: On the value of diatoms for tracing fast flow path connectivity from headwaters to meso-scale catchments. *Hydrological Processes*, 29(25), 5275–5289. <https://doi.org/10.1002/hyp.10628>
- Latron, J., & Gallart, F. (2007). Seasonal dynamics of runoff-contributing areas in a small mediterranean research catchment (Vallcebre, Eastern Pyrenees). *Journal of Hydrology*, 335(1–2), 194–206. <https://doi.org/10.1016/j.jhydrol.2006.11.012>
- Leach, J. A., Lidberg, W., Kuglerová, L., Peralta-Tapia, A., Ågren, A., & Laudon, H. (2017). Evaluating topography-based predictions of shallow lateral groundwater discharge zones for a boreal lake-stream system. *Water Resources Research*, 53(7), 5420–5437. <https://doi.org/10.1002/2016WR019804>
- Ledesma, J. L. J., Futter, M. N., Blackburn, M., Lidman, F., Grabs, T., Sponseller, R. A., ... Köhler, S. J. (2018). Towards an improved conceptualization of riparian zones in boreal forest headwaters. *Ecosystems*, 21(2), 297–315. <https://doi.org/10.1007/s10021-017-0149-5>
- Martínez-Carreras, N., Hissler, C., Gourdol, L., Klaus, J., Juilleret, J., Iffly, J. F., & Pfister, L. (2016). Storage controls on the generation of double peak hydrographs in a forested headwater catchment. *Journal of Hydrology*, 543, 255–269. <https://doi.org/10.1016/j.jhydrol.2016.10.004>



- McDonnell, J. J., Owens, I. F., & Stewart, M. K. (1991). A case study of shallow flow paths in an steep zero-order basin. *Water Resources Bulletin*, 27(4), 679–685.
- McGlynn, B. L., & McDonnell, J. J. (2003). Quantifying the relative contributions of riparian and hillslope zones to catchment runoff. *Water Resources Research*, 39(11), 1310. <https://doi.org/10.1029/2003WR002091>
- Mengistu, S. G., & Spence, C. (2016). Testing the ability of a semi-distributed hydrological model to simulate contributing area. *Water Resources Research*, 52(6), 4399–4415. <https://doi.org/10.1002/2016WR018760>
- Moragues-Quiroga, C., Juilleret, J., Gourdol, L., Pelt, E., Perrone, T., Aubert, A., ... Hissler, C. (2017). Genesis and evolution of regoliths: Evidence from trace and major elements and Sr-Nd-Pb-U isotopes. *Catena*, 149, 185–198. <https://doi.org/https://doi.org/10.1016/j.catena.2016.09.015>
- Myrabbø, S. (1997). Temporal and spatial scale of response area and groundwater variation in till. *Hydrological Processes*, 11(14), 1861–1880. [https://doi.org/10.1002/\(sici\)1099-1085\(199711\)11:14<1861::aid-hyp535>3.0.co;2-p](https://doi.org/10.1002/(sici)1099-1085(199711)11:14<1861::aid-hyp535>3.0.co;2-p)
- Niedda, M., & Pirastru, M. (2014). Field investigation and modelling of coupled stream discharge and shallow water-table dynamics in a small Mediterranean catchment (Sardinia). *Hydrological Processes*, 28(21), 5423–5435. <https://doi.org/10.1002/hyp.10016>
- O'Loughlin, E. M. (1987). Prediction of surface saturation zones in natural catchments by topographic analysis. *Water Resources Research*, 23(8), 1709–1709. <https://doi.org/10.1029/wr023i008p01709>
- Ocampo, C. J., Oldham, C. E., Sivapalan, M., & Turner, J. V. (2006). Hydrological versus biogeochemical controls on catchment nitrate export: A test of the flushing mechanism. *Hydrological Processes*, 20(20), 4269–4286. <https://doi.org/10.1002/hyp.6311>
- Pfister, L., Iffly, J. François, Hoffmann, L., & Humbert, J. (2002). Use of regionalized stormflow coefficients with a view to hydroclimatological hazard mapping. *Hydrological Sciences Journal*, 47(3), 479–491. <https://doi.org/10.1080/02626660209492948>
- Pfister, L., McDonnell, J. J., Hissler, C., & Hoffmann, L. (2010). Ground-based thermal imagery as a simple, practical tool for mapping saturated area connectivity and dynamics. *Hydrological Processes*, 24(May), 3123–3132. <https://doi.org/10.1002/hyp.7840>
- Phillips, R. W., Spence, C., & Pomeroy, J. W. (2011). Connectivity and runoff dynamics in heterogeneous basins. *Hydrological Processes*, 25(19), 3061–3075. <https://doi.org/10.1002/hyp.8123>
- Ploum, S. W., Leach, J. A., Kuglerová, L., & Laudon, H. (2018). Thermal detection of discrete riparian inflow points (DRIPs) during contrasting hydrological events. *Hydrological Processes*, 32(19), 3049–3050. <https://doi.org/10.1002/hyp.13184>
- Rodhe, A., & Seibert, J. (1999). Wetland occurrence in relation to topography: A test of topographic indices as moisture indicators. *Agricultural and Forest Meteorology*, 98–99, 325–340. [https://doi.org/10.1016/S0168-1923\(99\)00104-5](https://doi.org/10.1016/S0168-1923(99)00104-5)
- Rodriguez, N. B., & Klaus, J. (2019). Catchment travel times from composite StorAge selection functions representing the superposition of streamflow generation processes. *Water Resources Research*, 55, 9292–9314. <https://doi.org/10.1029/2019WR024973>
- Roulet, N. T. (1990). Hydrology of a headwater basin wetland. *Hydrological Processes*, 4(April), 387–340.
- Scaini, A., Audebert, M., Hissler, C., Fenicia, F., Gourdol, L., Pfister, L., & Beven, K. J. (2017). Velocity and celerity dynamics at plot scale inferred from artificial tracing experiments and time-lapse ERT. *Journal of Hydrology*, 546, 28–43. <https://doi.org/10.1016/j.jhydrol.2016.12.035>
- Schwab, M. P., Klaus, J., Pfister, L., & Weiler, M. (2018). Diel fluctuations of viscosity-driven riparian inflow affect streamflow DOC concentration. *Biogeosciences*, 15(7), 2177–2188. <https://doi.org/10.5194/bg-15-2177-2018>
- Seibert, S. P., Jackisch, C., Ehret, U., Pfister, L., & Zehe, E. (2017). Unravelling abiotic and biotic controls on the seasonal water balance using data-driven dimensionless diagnostics. *Hydrology and Earth System Sciences*, 21(6), 2817–2841. <https://doi.org/10.5194/hess-21-2817-2017>
- Selker, J., van de Giesen, N. C., Westhoff, M., Luxemburg, W., & Parlange, M. B. (2006). Fiber optics opens window on stream dynamics. *Geophysical Research Letters*, 33(24), 27–30. <https://doi.org/10.1029/2006GL027979>
- Silasari, R., Parajka, J., Ressler, C., Strauss, P., & Blöschl, G. (2017). Potential of time-lapse photography for identifying saturation area dynamics on agricultural hillslopes. *Hydrological Processes*, 31(21), 3610–3627. <https://doi.org/10.1002/hyp.11272>
- Soulsby, C., Birkel, C., & Tetzlaff, D. (2016). Modelling storage-driven connectivity between landscapes and riverscapes: Towards a simple framework for long-term ecohydrological assessment. *Hydrological Processes*, 30(14), 2482–2497. <https://doi.org/10.1002/hyp.10862>
- Stieglitz, M. (2003). An approach to understanding hydrologic connectivity on the hillslope and the implications for nutrient transport. *Global Biogeochemical Cycles*, 17(4), 1–15. <https://doi.org/10.1029/2003GB002041>
- Tanaka, T., Yasuhara, M., Sakai, H., & Marui, A. (1988). The Hachioji Experimental Basin study—Storm runoff processes and the mechanism of its generation. *Journal of Hydrology*, 102(1–4), 139–164. [https://doi.org/10.1016/0022-1694\(88\)90095-9](https://doi.org/10.1016/0022-1694(88)90095-9), 164
- Tetzlaff, D., Birkel, C., Dick, J., Geris, J., & Soulsby, C. (2014). Storage dynamics in hypopedological units control hillslope connectivity, runoff generation, and the evolution of catchment transit time distributions. *Water Resources Research*, 50(2), 969–985. <https://doi.org/10.1002/2013WR014147>
- Tetzlaff, D., McDonnell, J. J., Uhlenbrook, S., McGuire, K. J., Bogaart, P. W., Naef, F., ... Soulsby, C. (2008). Conceptualizing catchment processes: Simply too complex? *Hydrological Processes*, 22(11), 1727–1730. <https://doi.org/10.1002/hyp.7069>
- Tetzlaff, D., Soulsby, C., Waldron, S., Malcolm, I. A., Bacon, P. J., Dunn, S. M., ... Youngson, A. F. (2007). Conceptualization of runoff processes using a geographical information system and tracers in a nested mesoscale catchment. *Hydrological Processes*, 21(10), 1289–1307. <https://doi.org/10.1002/hyp.6309>
- van Meerveld, H. J., Seibert, J., & Peters, N. E. (2015). Hillslope-riparian-stream connectivity and flow directions at the Panola Mountain research watershed. *Hydrological Processes*, 29(16), 3556–3574. <https://doi.org/10.1002/hyp.10508>
- Vidon, P. G. F., & Hill, A. R. (2004). Landscape controls on the hydrology of stream riparian zones. *Journal of Hydrology*, 292(1–4), 210–228. <https://doi.org/10.1016/j.jhydrol.2004.01.005>
- von Freyberg, J., Radny, D., Gall, H. E., & Schirmer, M. (2014). Implications of hydrologic connectivity between hillslopes and riparian zones on streamflow composition. *Journal of Contaminant Hydrology*, 169, 62–74. <https://doi.org/10.1016/j.jconhyd.2014.07.005>
- Waddington, J. M., Roulet, N. T., & Hill, A. R. (1993). Runoff mechanisms in a forested groundwater discharge wetland. *Journal of Hydrology*, 147(1–4), 37–60. [https://doi.org/10.1016/0022-1694\(93\)90074-J](https://doi.org/10.1016/0022-1694(93)90074-J)
- Weill, S., Altissimo, M., Cassiani, G., Deiana, R., Marani, M., & Putti, M. (2013). Saturated area dynamics and streamflow generation from coupled surface-subsurface simulations and field observations. *Advances in Water Resources*, 59, 196–208. <https://doi.org/10.1016/j.advwatres.2013.06.007>
- Western, A. W., Grayson, R. B., Blöschl, G., Willgoose, G. R., & McMahon, T. A. (1999). Observed spatial organization of soil moisture and its relation to terrain indices. *Water Resources Research*, 35(3), 797–810. <https://doi.org/10.1029/1998WR900065>
- Wrede, S., Fenicia, F., Martínez-Carreras, N., Juilleret, J., Hissler, C., Krein, A., ... Pfister, L. (2014). Towards more systematic perceptual model development: A case study using 3 Luxembourgish catchments. *Hydrological Processes*, (1), n/a-n/a. <https://doi.org/10.1002/hyp.10393>

- Wrede, S., Fenicia, F., Martínez-Carreras, N., Juilleret, J., Hissler, C., Krein, A., ... Pfister, L. (2015). Towards more systematic perceptual model development: A case study using 3 Luxembourgish catchments. *Hydrological Processes*, 29(12), 2731–2750. <https://doi.org/10.1002/hyp.10393>
- Zehe, E., Lee, H., & Sivapalan, M. (2006). Dynamical process upscaling for deriving catchment scale state variables and constitutive relations for meso-scale process models. *Hydrology and Earth System Sciences*, 10(6), 981–996. <https://doi.org/10.5194/hess-10-981-2006>
- Zillgens, B., Merz, B., Kirnbauer, R., & Tilch, N. (2007). Analysis of the runoff response of an alpine catchment at different scales. *Hydrology and Earth System Sciences*, 11(4), 1441–1454. <https://doi.org/10.5194/hess-11-1441-2007>
- Zuocco, G., Penna, D., & Borga, M. (2018). Runoff generation in mountain catchments: Long-term hydrological monitoring in the Rio Vauz catchment, Italy. *Cuadernos de Investigación Geográfica*, 44(2), 397. <https://doi.org/10.18172/cig.3327>

**How to cite this article:** Antonelli M, Glaser B, Teuling AJ, Klaus J, Pfister L. Saturated areas through the lens: 1. Spatio-temporal variability of surface saturation documented through thermal infrared imagery. *Hydrological Processes*. 2020;1–23. <https://doi.org/10.1002/hyp.13698>

## APPENDIX A

Bibliography for the 30 studies considered for the review figure (Figure 1):

- Ali, G., Birkel, C., Tetzlaff, D., Soulsby, C., McDonnell, J. J., & Tarolli, P. (2013). A comparison of wetness indices for the prediction of observed connected saturated areas under contrasting conditions. *Earth Surface Processes and Landforms*, 39(3), 399–413. <https://doi.org/10.1002/esp.3506>

- Ambroise, B. (2016). Variable water-saturated areas and streamflow generation in the small Ringelbach catchment (Vosges Mountains, France): The master recession curve as an equilibrium curve for interactions between atmosphere, surface and ground waters. *Hydrological Processes*, 30(20), 3,560–3,577. <https://doi.org/10.1002/hyp.10947>

- Bari, M. A., Smettem, K. R. J., & Sivapalan, M. (2005). Understanding changes in annual runoff following land use changes: A systematic data-based approach. *Hydrological Processes*, 19(13), 2,463–2,479. <https://doi.org/10.1002/hyp.5679>

- Birkel, C., Tetzlaff, D., Dunn, S. M., & Soulsby, C. (2010). Towards a simple dynamic process conceptualization in rainfall-runoff models using multi-criteria calibration and tracers in temperate, upland catchments. *Hydrological Processes*, n/a-n/a. <https://doi.org/10.1002/hyp.7478>

- Blazkova, S., Beven, K. J., & Kulasova, A. (2002). On constraining TOPMODEL hydrograph simulations using partial saturated area information. *Hydrological Processes*, 16(2), 441–458. <https://doi.org/10.1002/hyp.331>

- Brun, C., Bernard, R., Vidal-Madjar, D., Gascuel-Oudou, C., Merot, P., Duchesne, J., & Nicolas, H. (1990). Mapping Saturated Areas With a Helicopter-Borne C-Band Scatterometer. *Water Resources Research*, 26(5), 945–955. <https://doi.org/10.1029/89wr03627>

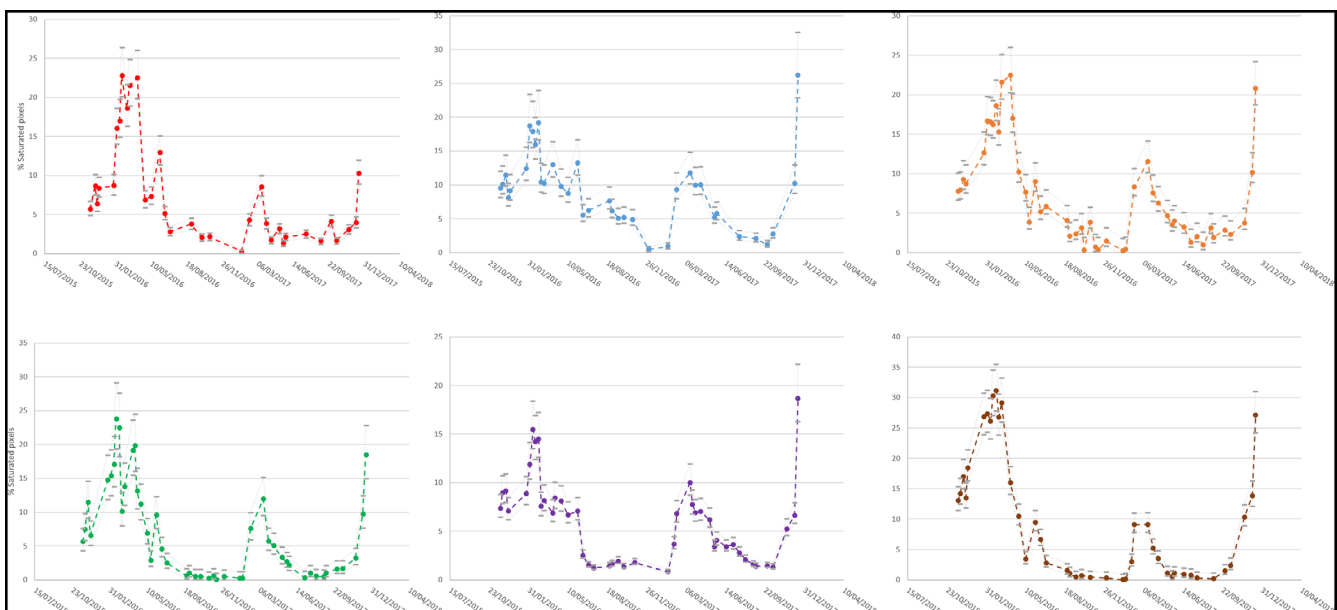


**FIGURE A1** Range of possible outcomes for the estimation of the percentage of saturated pixels for Areas L1, M1, M2, M3, R2, and R3. Coloured points and dashed lines refer to the optimal estimated saturation (cf. Figure 7 and optimal solution definition in Section 3.2). Grey dashes and dotted lines refer to the maximum and minimum estimated saturation (cf. Figure 7 and maximum and minimum estimated saturation definition in Section 3.2). Linear interpolations between the different observation dates are displayed as dashed and dotted lines and are meant to show the overall time series trend and might not reflect the actual saturation



- Buttle, J. M., & Sami, K. (1992). Testing the groundwater ridging hypothesis of streamflow generation during snowmelt in a forested catchment. *Journal of Hydrology*, 135(1–4), 53–72. [https://doi.org/10.1016/0022-1694\(92\)90080-F](https://doi.org/10.1016/0022-1694(92)90080-F).
- Chabot, D., & Bird, D. M. (2014). Small unmanned aircraft: Precise and convenient new tools for surveying wetlands. *Journal of Unmanned Vehicle Systems*, 01(01), 15–24. <https://doi.org/10.1139/juvs-2013-0014>
- Coles, A. E., & McDonnell, J. J. (2018). Fill and spill drives runoff connectivity over frozen ground. *Journal of Hydrology*, 558, 115–128. <https://doi.org/10.1016/j.jhydrol.2018.01.016>
- Creed, I. F., Sanford, S. E., Beall, F. D., Molot, L. A., & Dillon, P. J. (2003). Cryptic wetlands: Integrating hidden wetlands in regression models of the export of dissolved organic carbon from forested landscapes. *Hydrological Processes*, 17(18), 3,629–3,648. <https://doi.org/10.1002/hyp.1357>
- de Alwis, D. a., Easton, Z. M., Dahlke, H. E., Philpot, W. D., & Steenhuis, T. S. (2007). Unsupervised classification of saturated areas using a time series of remotely sensed images. *Hydrology and Earth System Sciences*, 11(5), 1,609–1,620. <https://doi.org/10.5194/hess-11-1609-2007>
- Devito, K. J., Creed, I. F., & Fraser, C. J. D. (2005). Controls on runoff from a partially harvested aspen-forested headwater catchment, Boreal Plain, Canada. *Hydrological Processes*, 19(1), 3–25. <https://doi.org/10.1002/hyp.5776>
- Dunne, T., Moore, T. R., & Taylor, C. H. (1975). Recognition and prediction of runoff-producing zones in humid regions. *Hydrological Sciences Bulletin*, 20(3), 305–327. [https://doi.org/10.1080/0022-1694\(1975\)20:3<305::AID-HYP576>3.0.CO;2-G](https://doi.org/10.1080/0022-1694(1975)20:3<305::AID-HYP576>3.0.CO;2-G)
- Franks, S. W., Gineste, P., Beven, K. J., & Merot, P. (1998). On constraining the predictions of a distributed model: The incorporation of fuzzy estimates of saturated areas into the calibration process. *Water Resources Research*, 34(4), 787–797. <https://doi.org/10.1029/97WR03041>
- Gineste, P., Puech, C., & Mérot, P. (1998). Radar remote sensing of the source areas from the Coët-Dan catchment. *Hydrological Processes*, 12(2), 267–284. [https://doi.org/10.1002/\(SICI\)1,099-1,085\(199802\)12:2<267::AID-HYP576>3.0.CO;2-G](https://doi.org/10.1002/(SICI)1,099-1,085(199802)12:2<267::AID-HYP576>3.0.CO;2-G)
- Glaser, B., Klaus, J., Frei, S., Frentress, J., Pfister, L., & Hopp, L. (2016). On the value of surface saturated area dynamics mapped with thermal infrared imagery for modeling the hillslope-riparian-stream continuum. *Water Resources Research*, 52(10), 8,317–8,342. <https://doi.org/10.1002/2015WR018414>
- Grabs, T., Seibert, J., Bishop, K., & Laudon, H. (2009). Patterns of saturated areas: A comparison of the topographic wetness index and a dynamic distributed model. *Journal of Hydrology*, 373(1–2), 15–23. <https://doi.org/10.1016/j.jhydrol.2009.03.031>
- Güntner, A., Uhlenbrook, S., Seibert, J., & Leibundgut, C. (1999). Multi-criterial validation of TOPMODEL in a mountainous catchment. *Hydrological Processes*, 13(11), 1,603–1,620. [https://doi.org/10.1002/\(SICI\)1,099-1,085\(19990815\)13:11<1,603::AID-HYP830>3.0.CO;2-K](https://doi.org/10.1002/(SICI)1,099-1,085(19990815)13:11<1,603::AID-HYP830>3.0.CO;2-K)
- Güntner, Andreas, Seibert, J., & Uhlenbrook, S. (2004). Modeling spatial patterns of saturated areas: An evaluation of different terrain indices. *Water Resources Research*, 40(5), 1–19. <https://doi.org/10.1029/2003WR002864>
- Inamdar, S. P., & Mitchell, M. J. (2007). Contributions of riparian and hillslope waters to storm runoff across multiple catchments and storm events in a glaciated forested watershed. *Journal of Hydrology*, 341(1–2), 116–130. <https://doi.org/10.1016/j.jhydrol.2007.05.007>
- Kulasova, A., Beven, K. J., Blazkova, S. D., Rezacova, D., & Cajthaml, J. (2014). Comparison of saturated areas mapping methods in the Jizera Mountains, Czech Republic. *Journal of Hydrology & Hydromechanics*, 62(2), 160–168. <https://doi.org/10.2478/johh-2014-0002>
- Latron, J., & Gallart, F. (2007). Seasonal dynamics of runoff-contributing areas in a small mediterranean research catchment (Vallebre, Eastern Pyrenees). *Journal of Hydrology*, 335(1–2), 194–206. <https://doi.org/10.1016/j.jhydrol.2006.11.012>
- McDonnell, J. J., & Taylor, C. H. (1987). Surface and subsurface water contributions during snowmelt in a small precambrian shield Watershed, Muskoka, Ontario. *Atmosphere - Ocean*, 25(3), 251–266. <https://doi.org/10.1080/07055900.1987.9649274>
- Mengistu, S. G., & Spence, C. (2016). Testing the ability of a semi-distributed hydrological model to simulate contributing area. *Water Resources Research*, 52(6), 4,399–4,415. <https://doi.org/10.1002/2016WR018760>
- Pfister, L., McDonnell, J. J., Hissler, C., & Hoffmann, L. (2010). Ground-based thermal imagery as a simple, practical tool for mapping saturated area connectivity and dynamics. *Hydrological Processes*, 24(May), 3,123–3,132. <https://doi.org/10.1002/hyp.7840>
- Phillips, R. W., Spence, C., & Pomeroy, J. W. (2011). Connectivity and runoff dynamics in heterogeneous basins. *Hydrological Processes*, 25(19), 3,061–3,075. <https://doi.org/10.1002/hyp.8123>
- Rinderer, M., Kollegger, A., Fischer, B. M. C., Stähli, M., & Seibert, J. (2012). Sensing with boots and trousers—qualitative field observations of shallow soil moisture patterns. *Hydrological Processes*, 26(26), 4,112–4,120. <https://doi.org/10.1002/hyp.9531>
- Roulet, N. T. (1990). Hydrology of a headwater basin wetland. *Hydrological Processes*, 4(April), 387–40.
- Silasari, R., Parajka, J., Ressler, C., Strauss, P., & Blöschl, G. (2017). Potential of time-lapse photography for identifying saturation area dynamics on agricultural hillslopes. *Hydrological Processes*, 31(21), 3,610–3,627. <https://doi.org/10.1002/hyp.11272>
- Tanaka, T., Yasuhara, M., Sakai, H., & Marui, A. (1988). The Hachioji Experimental Basin Study - Storm runoff processes and the mechanism of its generation. *Journal of Hydrology*, 102(1–4), 139–164. [https://doi.org/10.1016/0022-1694\(88\)90095-9](https://doi.org/10.1016/0022-1694(88)90095-9)